BRNO UNIVERSITY OF TECHNOLOGY
VYSOKÉ UČENÍ TECHNICKÉ V BRNĚ

FACULTY OF MECHANICAL ENGINEERING
FAKULTA STROJNÍHO INŽENÝRSTVÍ

ENERGY INSTITUTE
ENERGETICKÝ ÚSTAV

HYDRAULIC DESIGN AND CFD SIMULATION OF IMPELLER WITH INTEGRATED INDUCER

HYDRAULICKÝ NÁVRH A CFD VÝPOČET OBĚŽNÉHO KOLA S INTEGROVANÝM INDUCEREM

MASTER'S THESIS
DIPLOMOVÁ PRÁCE

AUTHOR **Bc. PAVEL NOVOSAD**
AUTOR PRÁCE

SUPERVISOR **Ing. DAVID ŠTEFAN, Ph.D.**
VEDOUCÍ PRÁCE

BRNO 2023

BRNO UNIVERSITY OF TECHNOLOGY
FACULTY OF MECHANICAL ENGINEERING

Assignment Master's Thesis

Institut:	Energy Institute
Student:	**Bc. Pavel Novosad**
Degree programm:	Power and Thermo-fluid Engineering
Branch:	Fluid Engineering
Supervisor:	**Ing. David Štefan, Ph.D.**
Academic year:	2022/23

As provided for by the Act No. 111/98 Coll. on higher education institutions and the BUT Study and Examination Regulations, the director of the Institute hereby assigns the following topic of Master's Thesis:

Hydraulic design and CFD simulation of impeller with integrated inducer

Brief Description:

This topic is focused on the hydraulic design of an impeller with an integrated inducer and subsequent verification using CFD calculations. Currently, development projects related to the design of electrically driven pumps for fuel and oxidizer of rocket engines with thrust in the order of several tens of kN were taking place at our department. The projects are mostly related to the activities of the European Space Agency (ESA), where the goal is to design and manufacture electrically powered pumps using batteries as a power source. The requirements usually lead to a solution where the pump runs at very high speeds of 50,000 – 100,000 rpm and thus the dimensions of the hydraulic parts are very small.
Another factor is the required or guaranteed suction pressure, which, if insufficient, leads to the solution of a pump with an inducer. In most cases, the inducer is designed as a separate axial wheel placed in front of the main impeller. Considering the small dimensions, however, this may not be an advantageous solution, and therefore the goal of this thesis is to design an impeller with an "integrated" inducer, where the blades of the inducer form at the same time some of the blades of the impeller.

Master's Thesis goals:

The goal of this thesis is hydraulic design of centrifugal pump impeller with integrated inducer. This design variant will be compared with classical concept of separated inducer from the impeller and/or with concept without inducer. The new hydraulic design will be verified using CFD simulation.

Recommended bibliography:

GÜLICH, Johann Friedrich, 2020. Centrifugal Pumps [online]. 4. Cham: Springer International Publishing [cit. 2022-11-01]. ISBN 978-3-030-14787-7. Dostupné z: doi:10.1007/978-3-030-14788-4.

BLÁHA, Jaroslav a Karel BRADA. Příručka čerpací techniky. Praha: Vydavatelství ČVUT, 1997. ISBN 80-01-01626-9.

GWIASDA, Björn, Matthias MOHR a Martin BÖHLE, 2019. Investigations of Inducers Operating With High Rotational Speed. Journal of Fluids Engineering [online]. 141(4), 10 [cit. 2022-11-01]. ISSN 0098-2202. Dostupné z: doi:10.1115/1.4041730.

LUBINIECKY, Marek, 2018. Rocket engine inducer design optimisation to improve its suction performance. Delft, Netherland. Master Thesis. TU Delft. Vedoucí práce Dr. A. Cervone, Dr. C. Lettieri.

Deadline for submission Master's Thesis is given by the Schedule of the Academic year 2022/23

In Brno,

L. S.

doc. Ing. Jiří Pospíšil, Ph.D. Director of the Institute	doc. Ing. Jiří Hlinka, Ph.D. FME dean

Abstract

The main objective of this thesis is the hydraulic design of an oxidizer pump impeller for a rocket engine.

The introductory part of the thesis is dedicated to the research of essential terminology and phenomena influencing this design. This is followed by the iterative design of a radial pump, which is however susceptible to cavitation development. Then, the design of the axial stage pump is carried out to increase the radial stage inlet pressure. The design was based on an analytical 2D flow calculation and was subsequently modified using CFD analyses to improve the pump performance, efficiency, and cavitation stability.

The final step is to combine the two impellers into one, which due to its more compact dimensions, achieves higher efficiency and is easier to manufacture. For this impeller, assessments are carried out for strength failure, the occurrence of resonance, and susceptibility to cavitation development at low suction pressure.

Abstrakt

Cílem této práce je hydraulický návrh oběžného kola čerpadla okysličovadla pro raketový motor.

Úvodní část práce je věnována rešerši podstatných pojmů a jevů, které tento návrh ovlivňují. Následuje iterativní návrh radiálního čerpadla, které je ale náchylné na vznik kavitace. Poté je proveden návrh axiálního stupně čerpadla, který má navyšovat vstupní tlak do radiálního stupně. Návrh byl založen na analytickém výpočtu 2D proudění, který byl následně za pomoci CFD analýz modifikován pro zlepšení výkonu, účinnosti a kavitační stability čerpadla.

Finálním krokem je tyto dvě oběžné kola spojit do jednoho, které díky kompaktnějším rozměrům dosahuje vyšší účinnosti a je méně náročné na výrobu. Pro toto kolo jsou provedeny kontroly vůči meznímu stavu pružnosti, výskytu rezonance a náchylnosti na výskyt kavitace při nízkém sacím tlaku.

Keywords

centrifugal pump, inducer, cavitation, CFD

Klíčová slova

odstředivé čerpadlo, inducer, kavitace, CFD

Reference

NOVOSAD, Pavel. *Hydraulic design and CFD simulation of impeller with integrated inducer* [online]. Brno, 2023 [cit. 2023-05-26]. Available at: https://www.vut.cz/studenti/zav-prace/detail/149952. Master's thesis. Brno University of Technology, Faculty of Mechanical Engineering, Energy Institute. Supervisor Ing. David Štefan, Ph.D.

Rozšířený abstrakt

Cílem této práce bylo vytvořit hydraulický návrh oběžného kola elektrického čerpadla pro dopravu okysličovadla do raketového motoru. Čerpadlo je specifické tím, že musí být schopno provozu při nízkém tlaku čerpané kapaliny.

Pro rakety je velmi důležitou veličinou jejich hmotnost, jelikož jakákoliv přianá hmotnost výrazně zvyšuje práci, která musí být vynaložena, aby se raketa dopravila na oběžnou dráhu. Jednou z oblastí, kde je možné výrazně snížit hmotnost jsou nádrže paliva a okysličovadla. Většina palivových nádržích je přetlakových a aby tento tlak vydržely, potřebují silnější stěny. Čerpadlo navrhované v rámci této práce má být schopno pracovat při nižších tlacích, aby nádrže mohly mít tenší stěny a byly lehčí.

Byla proto provedena rešerše aktuálně používaných koncepcí raketových motorů, jejich paliva a prostředků, kterými je dopravováno. Dále byly představeny důvody, které vedou k vývoji elektricky napájených palivových čerpadel. Nakonec byl představen koncept, stanovující uspořádání navrhovaného čerpadla do fuknčního celku.

Jelikož hlavním problémem čerpadla bude zajištění provozu bez výskystu kavitace, byla provedena rešerše, která popisuje co to je kavitace, jak vzniká a jaký má vliv na hydraulické stroje. Zejména důležité je zmínění kde se kavitace vyskytuje, aby bylo možné jí předejít. Byly představeny charakteristiky odstředivých čerpadel, které jsou pro konstrukci oběžného kola podstatné a jak je lze ovlivnit.

K tomu aby byl potenciální návrh oběžného kola skutečně použitelný bylo potřeba jej přizpůsobit možnostem výrobní technologie a vlastnostem použitého materiálu. Byla proto provedena studie materiálů používaných pro výrobu oběžných kol, ze kterých byla následně zvolena pro výrobu superslitina niklu Inconel 718. Tento materiál se vyznačuje silnou korozní odolností, odolností vůči erozi a vysokou pevností.

Radiální stupně odstředivých čerpadel obecně disponují nejvyšší účinností. První návrh oběžného kola čerpadla byl proto radiální stupeň, který dosahoval požadovaných parametrů. Návrh vychází z analytických a empirických vztahů, které jsou vyvozeny z metod používachých v průmyslu. Tento návrh dále využívá úprav, které umožňují zvýšení jeho výkonu. Zejména se jedná o sklon odtokové hrany lopatek a o vhodnou volbu počtu lopatek.

Jelikož větší počet lopatek snižuje průtočnou plochu, zvyšuje se meridiální rychlost a klesá statický tlak kapaliny, byla zkoumána varianta lopatek vložených mezi hlavní lopatky v oblasti, kde už je tlak zvýšený dostatečně, aby nehrozil vznik kavitace. Poté byly porovnány varianta se třemi lopatkami a varianta s dalšími třemi vloženými mezilopatkami. Ukazuje se, že má význam použít více lopatek, neboť zajišťují vyšší účinnost, protože na každou lopatku připadá nižší nárust měrné energie, takže nejsou tolik přetěžovány. Navíc mělo oběžné kolo s více lopatkami širší provozní pásmo v závislosti na různém průtoku.

Problémem radiálního oběžného kola je silné zakřivení proudu kapaliny v blízkosti náběžné hrany lopatek. V této oblasti má kapalina nízký tlak a zahnutí proudu vytváří oblast, kde tlak dále poklesne a v této oblasti se může vytvořit silná kavitace, která naruší činnost čerpadla.

Tento problém se běžně řeší vložením axiálního stupně čerpadla před radiální stupeň. Axiální stupeň je méně náchylný na tvorbu podtlakové oblasti a navýší tlak čerpadla tak, aby

mohl radiální stupeň pracovat bez potíží. Bylo opět představeno několik geometrických úprav axiálních čerpadel, které slouží ke zvýšení jejich účinnosti a snížení potřebného sacího tlaku. Tyto úpravy byly následně použity při návrhu. Inducer využívá mírně rostoucí průměr náboje, který mu umožňuje využít odstředivého zrychlení kapaliny. Lopatky mají zahnutou a skloněnou náběžnou hranu, což snižuje vliv mezní vrsty kapaliny v přívodním potrubím. Lopatka je navíc tvarovaná jako aerodynamický profil, aby umožňovala účinnější zahnutí proudu kapaliny.

Na základě samostatného návrhu radiálního a axiálního stupně oběžného kola byly stanoveny geometrie vstupní a výstupní části čerpadla. Cílem práce bylo spojit tyto dvě části do jednoho celku a vytvořit oběžné kolo, které využívá výhod obou konstrukcí. Návrh lopatek tohoto oběžného kola byl poměrně náročný, neboť axiální i radiální stupně mají složitou geometrii lopatek a pro jejich vhodné provázání bylo potřeba značného ladění průběhu úhlu sklonu a úhlu opásání lopatek. Tyto úhly byly pro každou lopatku definovány v pěti vrstvách.

Pro kombinované oběžné kolo byla opět stanovena Q-H charakteristika, která ukázala že čerpadlo tohoto návrhu dosahuje vyšší maximální hydraulické účinnosti, ale má výrazně užší provozní pásmo, než čistě radiální stupeň.

Byla provedena dvoufázová simulace oběžného kola čerpadla, která zahrnovala fázovou přeměnu kapaliny v důsledku kavitace. Pomocí tohoto výpočtu byla numericky určena hodnota $NPSH_3$ v závislosti na průtoku čerpadla. Ukázalo se, že oběžné kolo je výrazně méně náchylné ke kavitaci, než se očekávalo na základě výsledků jednofázového výpočtu. Konstrukce čerpadla je schopna pracovat při vstupním tlaku o 27 procent nižším, než je požadováno.

Jelikož má oběžné kolo, vlivem předepsaných otáček velmi malé rozměry, jeho výroba je silně limitovaná. Zejména může být problematické dodržet požadovanou jakost povrchu na stěnách kanálů. Pro tento návrh byla proto provedena studie použitelnosti otevřené konstrukce oběžného kola. Byla provedena série simulací při použití geometrií s různě velkými spárami na konci lopatek. Z výsledků vyplynulo, že čerpadlo zpracovává tak vysoký nárust tlaku na tak krátké dráze, že je velmi výrazný rozdíl tlaků na tlačné a sací straně lopatky. A vzhledem k tomu, že na výstupu z oběžného kola má lopatka výšku pouze 1,56 milimetru, velké množství čerpané kapaliny obtéká lopatku z tlakové strany na sací a čerpadlo tím výzrazně ztrácí dopravní výšku.

Pro výsledný návrh byla nakonec provedena napjatostní analýza pro kontrolu vůči meznímu stavu pružnosti a modální analýza pro stanovení náchylnosti návrhu k rezonančnímu zesílení kmitání. Ukázalo se, že oběžného kolo se ani nepřibližuje riziku výskytu plastické deformace a vlastní frekvence lopatek nebudou při běžném provozu buzeny.

Výsledný návrh čerpadla je tedy použitelný ve variantě obsahující krycí disk. Je známa Q-H charakteristika a kavitační charakteristika. Čerpadlo splňuje požadované parametry a je schopno provozu i z hlediska napětí a rezonance. Problém ale nastává u varianty s otevřeným oběžným kolem, protože v tomto případě není čerpadlo schopno dodat požadovanou dopravní výšku, pokud bude spára na konci lopatek větší, než 0.1 milimetru. V tomto směru vyžaduje návrh další práci a jako nejvhodnější volba se jeví možnost krycího disku pouze v radiální části oběžného kola, přičemž axiální část bude otevřená.

Hydraulic design and CFD simulation of impeller with integrated inducer

Declaration

I hereby declare that this Master's thesis was prepared as an original work by the author under the supervision of Ing. David Štefan, Ph.D., with the use of listed sources.

.....
Pavel Novosad
May 29, 2023

Acknowledgements

I would like to express my deep gratitude to my supervisor Ing. David Štefan, Ph.D. for his guidance and valuable advice when numerous problems arose. I would also like to thank my family and friends for their support throughout my studies.

Contents

Chapter 1

Introduction

Hydrodynamic pumps have been historically the dominant design for conveying fuel and oxidizer to jet and rocket engine nozzles due to their simplicity, reliability, and stability of fluid transport.

However, the disadvantage of centrifugal pumps is often the development of low-pressure regions near their inlet. This area is susceptible to cavitation and a decline in pumping characteristics. A possible solution to this problem is to maintain the pumped fluid under pressure. However, this has the effect of increasing the strength of the reservoirs, which usually entails an increase in the thickness of their walls, as transporting mass into space is expensive, there is a strong effort underway in rocket design to minimize the weight of the craft.

One solution is to use pumps capable of operating at low suction pressures. This can significantly reduce the weight of the tanks. At the same time, there is an effort to reduce the weight of the pump itself. This applies to both the hydraulic and propulsion parts.

Thanks to current trends in the development of electric battery cells of higher energy density, it turns out that when a sufficiently efficient and powerful cooling system is designed, it is possible to create very powerful electric motors of small dimensions. Such motors operate at very high speeds and have low torque.

The advantage of centrifugal pumps is that their design can be adapted to different drive parameters. One of the disadvantages of high pump speeds is the increased susceptibility to cavitation at the suction. It is, therefore, not possible to use a pump with conventional radial geometry. This problem is commonly solved by installing the axial stage to increase the pressure at the inlet of the radial stage.

This thesis aims to design a pump impeller that connects these two stages and consists of both axial and radial portions. Combining these two portions is expected to reduce turbulence at the inlet of the radial stage, increase efficiency, reduce the impeller dimensions, and reduce the deflection in the cover disc seal area.

Chapter 2

Rocket engines

The chemical rocket engine is classified as a reaction propulsion system. This means it uses a reaction force to develop thrust to compensate for the change in momentum of the flue gases. The fuel is fed into the nozzle where it is burned. This produces gases at high temperatures, and therefore, at the speed of sound. The flue gases are then directed oppositely to the desired thrust direction. It is possible to accelerate the exhaust gas above the speed of sound by properly designing the shape of the divergent combustion nozzle.

Unlike jet engines, rocket engines do not use atmospheric air, but carry a supply of oxidizer. This is an added weight compared to jet engines, but it allows operation outside of oxygen-containing environments.

2.1 Rocket fuel types

Several types of rocket engines are characterized by their design and fuel being used. The main differences are the fuel state and whether the fuel and oxidizer are stored separately. These designs offer a range of prices, performance, and thrust controllability.

2.1.1 Solid-propellant

A solid-propellant rocket engine is the simplest engine design currently used for rocket propulsion and its scheme can be seen in Figure 2.1. The earliest rockets used gunpowder as fuel and were used by Arabs and Chinese since the 13th century. It was the only way to design rockets until the 20th century when liquid propellant rockets began offering more efficient and controllable combustion. [20]

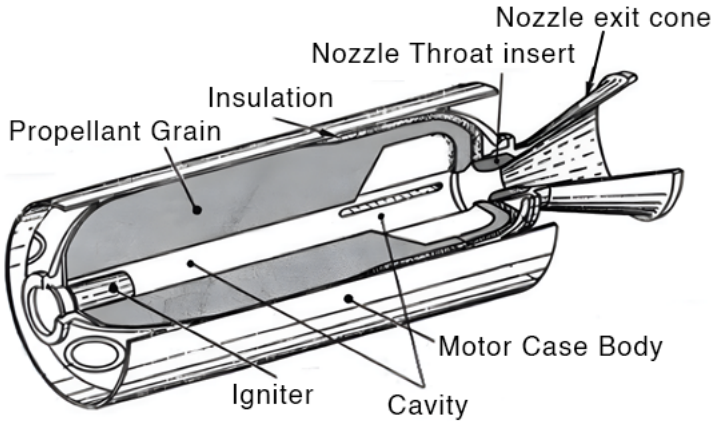

Figure 2.1: Solid rocket booster construction scheme [25]

Solid fuel is the most common propulsion type for hobby and amateur rocketry as well as for strap-on rocket boosters for the take-off of large rockets. These boosters are used at the launch of the rocket to overcome the majority of aerodynamic friction and to give the rocket an initial speed. Increasing the rocket's payload capacity, and are then dropped off the main rocket to reduce weight.

The benefits of solid-fuel rockets are that they are very reliable to launch and that they can last in storage for an extended period of time without significant propellant degradation. This makes them convenient for military applications such as missiles. Lower specific impulse makes solid-fuel rockets not ideal for the main body of the space rocket. They are, however, in some cases used for transporting small payloads of under 2 tonnes to low Earth orbit. Many of these rockets are based on repurposed intercontinental ballistic missiles. [19]

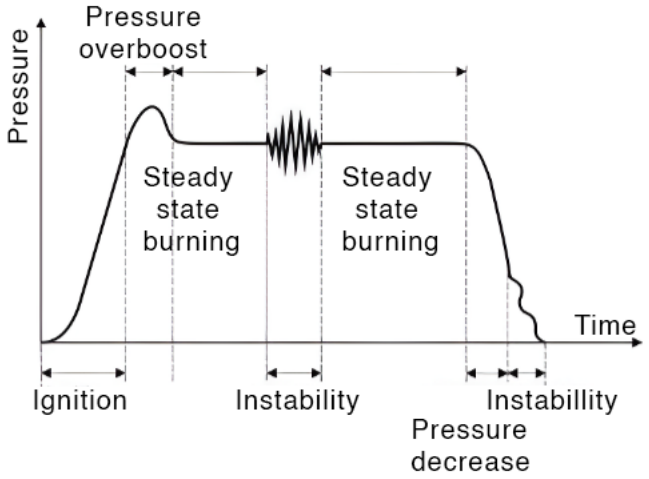

Figure 2.2: Solid booster thrust development with time of operation [41]

Electric solid propellants (ESP) are solid propellants whose combustion can be ignited and throttled by the application of electric current. This removes a major flaw of conventional

solid propellants, which once ignited burn at a steady rate as shown in Figure 2.2 and are difficult to control and extinguish. This solution requires no moving parts and is very reliable since the propellant is insensitive to flames and electrical sparks. [35]

2.1.2 Hybrid-propellant

Since most chemical rocket engines require at least two reacting media, the hybrid-propellant engine type utilizes one propellant in solid form and the other in liquid form. This design path can then be further various types as shown in Figure 2.3. The standard hybrid engine implementation consists of a fuel grain cast into the combustion chamber. The fuel is then cured and gains its solid structure. The liquid oxidizer is stored in a separate tank. When the engine is operating, the oxidizer is then injected into the combustion chamber. [5]

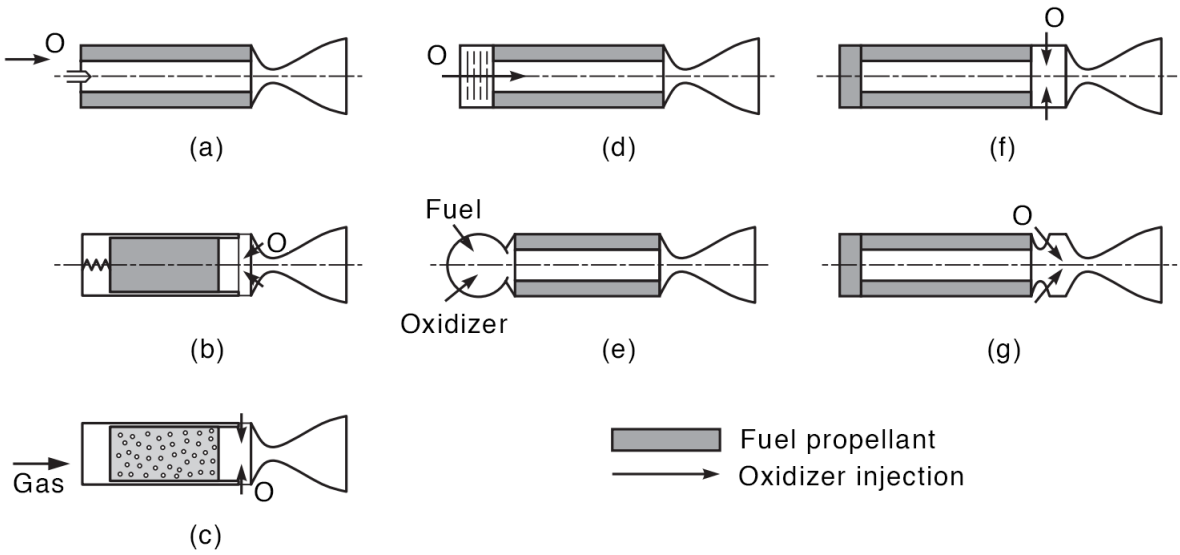

Figure 2.3: Typical hybrid motor concepts [5]: (a) liquid-solid reaction: head injection; (b) solid feed; (c) gel feed; (d) gas-solid reaction: monopropellant gas generator; (e) bi-propellant gas generator; (f) liquid gas reaction: aft oxidizer injection; and (g) aft Venturi injection

Depending on the type of fuel being used, the solid state can also be reached by freezing the fuel in the case of ethylene, or by creating a gel-like fuel consistency and keeping it in place by an internal matrix. The inverse-hybrid motor concept utilizes liquid fuel and solid oxidizer grain. The design is largely similar to that using solid fuel and a liquid oxidizer, but this design has proved not to be feasible with current oxidizer production technologies. A significant weakness of solid oxidizers is their reactivity, which makes them dangerous to operate. [5]

Hybrid propulsion requires the cooperation of two different engineering technologies. These technologies do not work reliably well together currently, but could theoretically provide multiple benefits when compared to solid or liquid fuel-propelled rockets. Solid fuel in hybrid

systems has a lower density than the fuel used in solid motors. This weight reduction can offset the weight added to accommodate liquid oxidizer storage and transportation system. With further development in fuel grain design, oxidizer injection, and fuel grain formulation, the combustion efficiency could be higher than that of solid and liquid-powered engines. Recent tests measured combustion efficiency of up to 91 percent. All hybrid fuels are considered inert and can be transported using normal shipping techniques without any additional safety requirements. This is a large benefit compared to solid propellants, whose handling is a hazardous operation requiring special handling considerations increasing the production cost due to safety requirements. [5]

2.1.3 Monopropellant

A monopropellant is a chemical compound, that can be used as rocket propulsion fuel while not requiring a separate oxidizer. This rocket engine design utilizes energy contained within the molecular bonds of the fuel. The most commonly used fuel is hydrazine. Hydrazine is a strong reducing agent and decomposes rapidly when in contact with a catalyst in the form of aluminum oxide coated with iridium. This decomposition is highly exothermic and produces a gas mixture of nitrogen, hydrogen, and ammonia at a temperature of 1000 $^{\circ}C$. Another monopropellant is 90 percent hydrogen peroxide, which is self-decomposing at high temperatures or when in contact with a catalyst. [44, 12]

Monopropellant engines are not very efficient, however, are being often used due to their simplicity and reliability. They can be as small as 10 millimeters in diameter and are able to be repeatedly ignited and shut off by simple valve opening. They are often employed as the attitude control motors for satellites and space probes. Four to twenty thrusters are often installed on the vessel, which are then controlled by the computer to exert exact pulses. These can be as short as a few milliseconds. [44]

2.1.4 Biopropellant

Biopropellant rocket engines create thrust by utilizing the combustion of fuel and oxidizer. Each is stored separately in liquid form. Because both fuel and oxidizer are injected into the thrust chamber by pumps, precise mixture control is possible, enabling more efficient combustion when compared to solid and hybrid rocket engines. This, however, comes with a cost in form of higher complexity, cost, and weight, as can be seen in Figure 2.4. [39]

A biopropellant rocket engine can be repeatedly reignited. This enables the possibility of testing each engine prior to use. Whereas for solid rocket motor, complex quality control must be implemented during manufacturing to ensure reliability. Depending on the vessel type the biopropellant engine can be reused for multiple flights. This is currently a large topic of development for companies like SpaceX, Blue Origin, and Virgin Galactic, but was also utilized in the past on the NASA's Space Shuttle. [22]

To keep lightweight tankage and vehicle structure, a lightweight turbopumps and electric pumps are used to pump propellants into the combustion chamber. These are further discussed in Chapter 3. Biopropellant rocket engines provide the highest specific impulse

currently available while providing thrust-to-weight ratios of up to 180:1 with the vacuum version of SpaceX Merlin 1D.

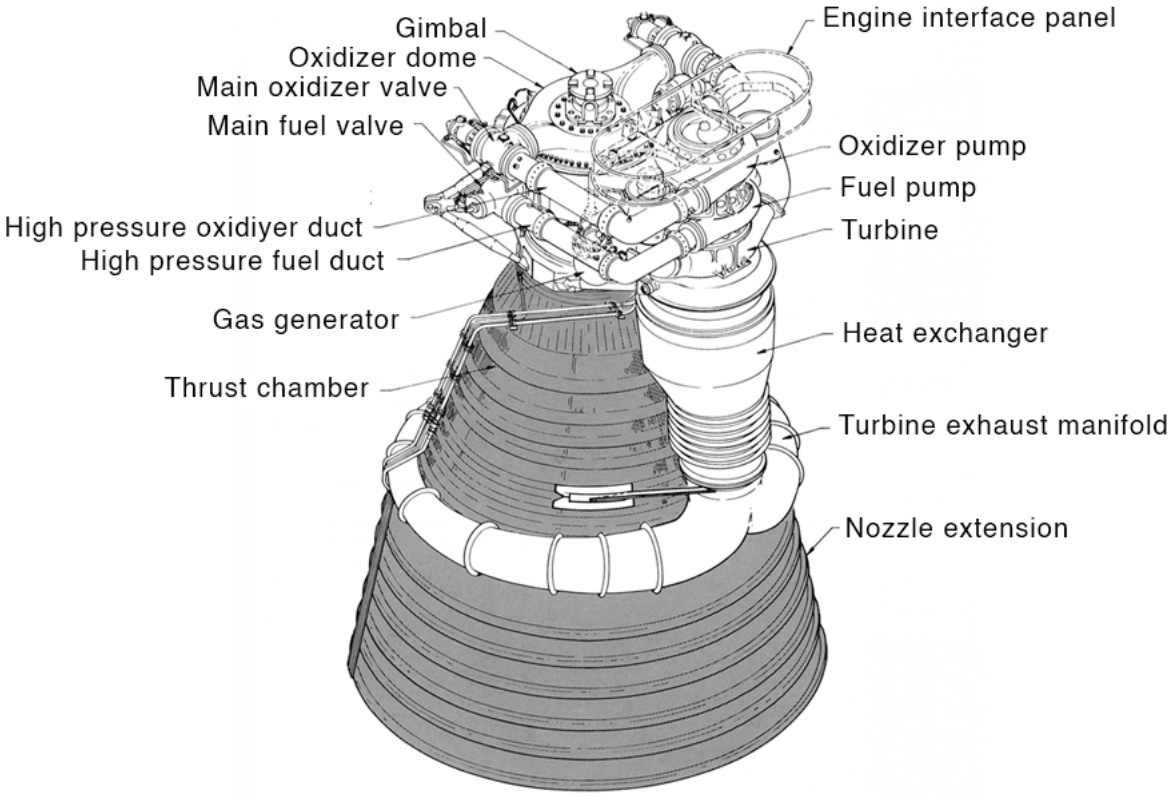

Figure 2.4: Liquid propellant rocket engine construction scheme

The propellants are introduced into the combustion chamber at high pressure of 2-20 MPa. Thrust chamber injectors require this to properly atomize incoming propellant and to provide high-pressure drop decoupling the flow through the fuel lines from the natural fluctuations in chamber pressure that occur during the combustion process. Insufficient pressure drop in the injectors can cause unsteady combustion and oscillations in thrust chamber pressure, which can damage the engine. This is mainly problematic during the ignition process. [39, 22]

For correct stable combustion, fast vaporization of liquid propellants is necessary. This is ensured by correct injector design and by using liquid propellant as cooing fluid for the thrust nozzle jacket. The jacket is manufactured out of welded or 3D-printed pipes, through which flows the propellant. This ensures the nozzle does not melt, and the propellant is heating closer to its boiling point. When it then enters the combustion chamber, it cools the combustion less and reacts quicker. [22]

Liquid fueled rocket engines can be powered by a large spectrum of propellants, some of witch are, along with their Ideal specific impulse, shown in Figure 2.5. The most prominent being combination of liquid oxygen with liquid hydrogen or liquid methane. These propellants are classified as cryogenic and to be stored in liquid form, they must be kept at low

temperatures around -250 $^{\circ}C$. They provide the highest specific impulse. Liquid methane is especially attractive to reusable launch systems, since its higher density allows for its use of smaller engines. Another historically used propellant combination is liquid oxygen with kerosene or ethanol. Ethanol was used in German World War II rocketry, mainly on V-2. Kerosene was then used on first stage of NASA's Apollo program rocket Saturn V. One of the more modern propellant combinations is 90 percent hydrogen peroxide as oxidizer with kerosene being used as fuel. This propellants have the benefit of being storable for long periods of time at relatively high temperature. They are also environmentally friendly and therefore have lower development cost. Ignition catalyst is often dispersed in the kerosene to provide fast and efficient combustion of up to 95 percent. [28, 39]

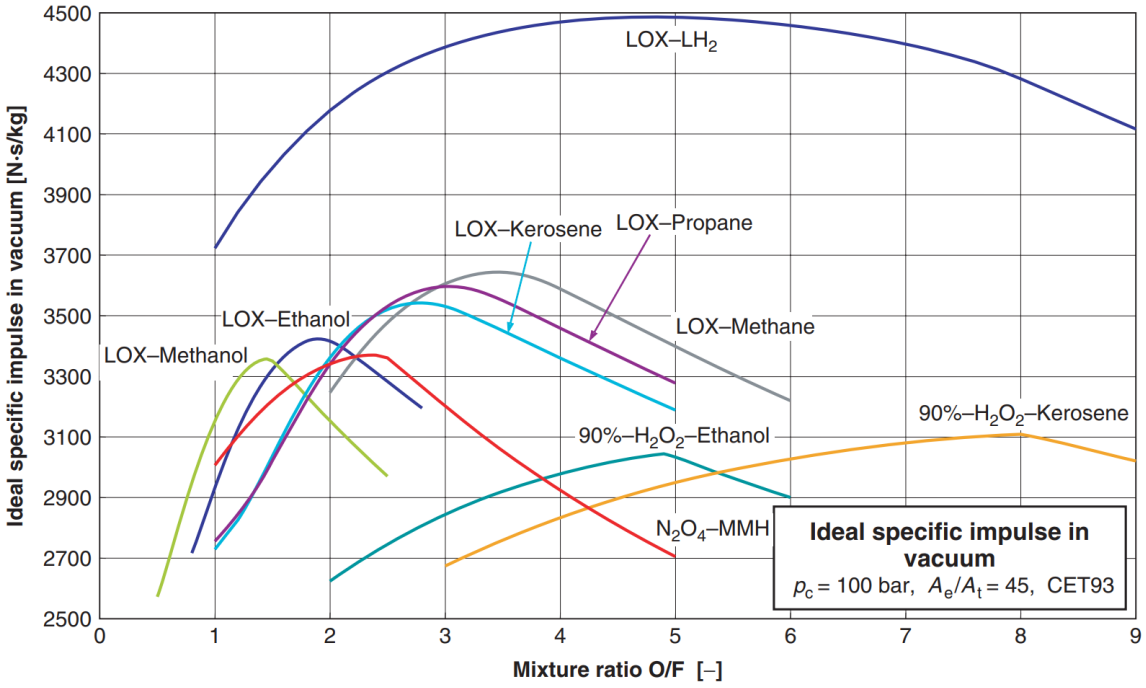

Figure 2.5: Ideal specific impulse of various rocket fuel and oxidizer combinations [44]

2.1.5 Gas-gas

One of the modern development avenues in rocket engine design are engines using both oxidizer and fuel in gaseous form. These engines will have relatively low thrust to weight ratio, but will be very simple and could replace current monopropellant attitude control motors as they can utilize main propellant tanks. Liquid propellant tanks eventually heat up and need to be vented. This vented propellant would then be used in gas thrusters for reaction control system. [17]

SpaceX have developed gaseous thrusters based on methane and oxygen, which are currently employed on SpaceX Starship. Their main purpose there is to replace main Raptor engines for the final „tenths of meters" of any lunar landing as well as take off. They are located in the middle of the body of the spacecraft to eliminate lunar surface erosion. [29]

Chapter 3

Propellant pumps

The majority of liquid-propellant rocket engines utilize forced propellant induction. This can be achieved by using pressurized propellant and oxidizer tanks or using a mechanical pump. Since mass is an important factor when designing a rocket, it is beneficial to reduce the weight of large parts, such as tanks, by installing a pump and lowering the required tank pressure.

Since rocket engines utilize stable combustion, they require a continuous propellant supply. However, the design of propellant injectors often requires high propellant pressure to provide the right stream dispersion. As a result of this, lightweight high-speed centrifugal pumps are the most commonly used design. A well-designed turbopump delivers the intended propellant flow at the intended discharge pressure and the mixture ratio is reliable and runs at the highest practical energy efficiency.

The problem with designing centrifugal pumps of such high speeds is the area of low pressure at the suction orifice of the pump, where cavitation can develop. This can significantly influence pump characteristics and can prevent its function altogether. Even if the pump operates with the cavitation region developed, the cavitation-produced bubbles downstream endanger the propellant nozzles function, which can lead to thrust chamber failure. This problem is solved by implementing an axial stage pump called an „inducer“ upstream of the main radial impeller. Inducer is less susceptible to cavitation development and can increase static pressure at the inlet of the radial impeller. This is usually done by increasing the swirl velocity of the fluid in the inducer and then decreasing it in stator deswirl vanes, where the pressure increases based on energy conservation law. [39]

3.1 Turbo pump

A turbopump is a high-speed machine, shown in Figure 3.1, consisting of a gas turbine and one or two centrifugal pumps. The gas turbine is driven by propellant combustion in a secondary combustion chamber. This solution can be very space efficient and light. Because of their high speed, turbopumps must be designed in such a way that does not cause any significant vibration nor are affected by external vibrations. Since engines are throttleable, it is important for the pump to be able to function under all operating conditions. These include different propellant temperatures, acceleration in various directions, and start and

stop transients. Bearings and seals must be adequately cooled by small secondary propellant flows to prevent malfunction. However, unexpected leaks in seals can not be tolerated. [39]

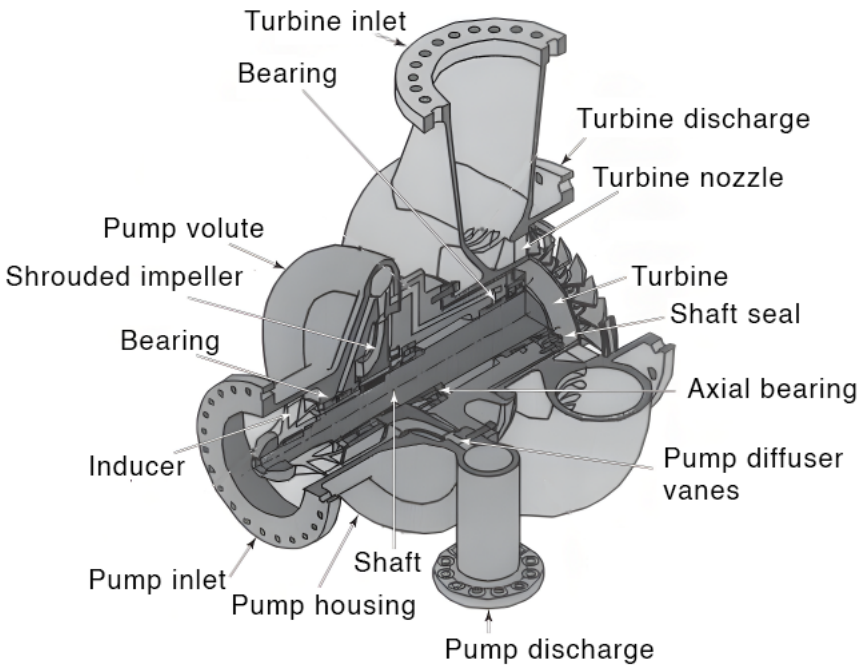

Figure 3.1: Rocket engine turbo pump construction scheme

3.2 Electric pump

As space industry aims towards private corporations manufacturing and operation, faster and cheaper ways of rocket design are being researched. One of the areas of interest is engine propellant distribution. Pressurised tanks and turbopumps are still the norm, altough turbopump development time and cost are a huge factor pushing towards use of electric pumps. Their most attractive features are the simplicity and controlability of the propellant supply system. Electrically driven propellant supply system scheme is shown in Figure 3.2, and consists of hydraulic pump, modern brushless DC motor, an invertor, and battery. [40, 32, 23]

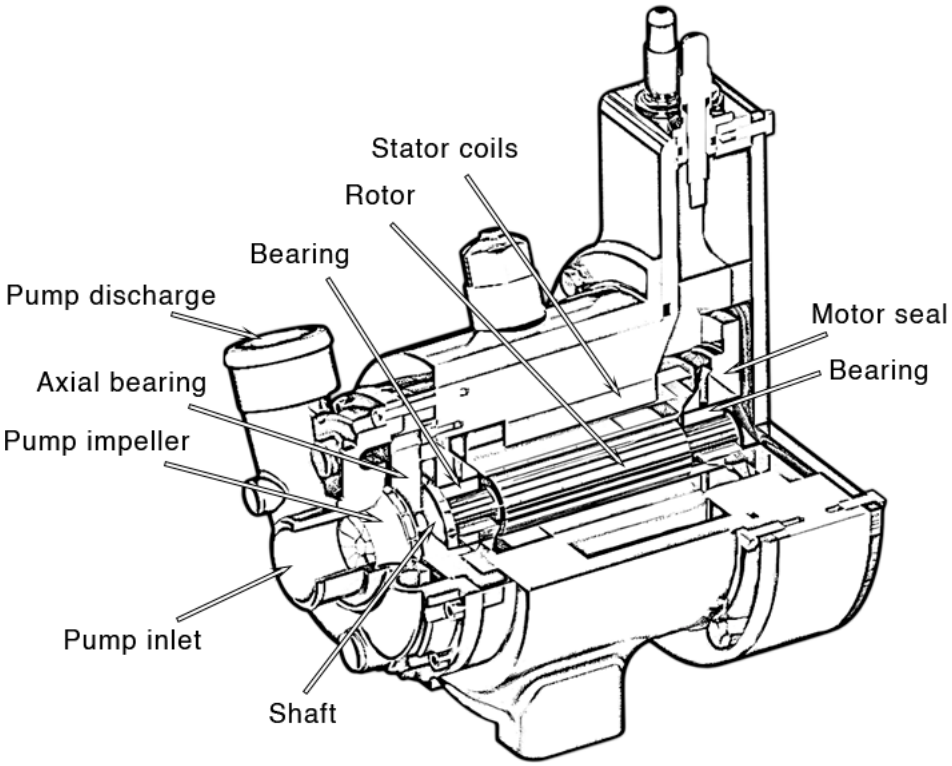

Figure 3.2: Electrical oxidizer pump construction scheme [2]

Current trends in electric motors allow the design of high-speed motors capable of speed at over a hundred thousand revolutions per minute. It is often impossible to cool these motors with common means. A commonly utilized solution is designing a hydraulic part without backdisc seal and having a rotor submerged in the propellant. This throughflow inside the motor is very effective at removing heat. Nonetheless, these solutions bring larger hydraulic losses of flow through the thin gap between the electric rotor and stator, thus increasing power demand. Another key issue is designing the heat transfer so that the propellant remains liquid everywhere and does not start to boil. The heated propellant is then guided back into the propellant tank. [40, 45]

The main limiting factor of electrically powered propellants is the battery's energy density. As of now, electric pumps can have benefits when used on engines with a maximum thrust of 30 kilonewtons. Batteries on larger engines would significantly reduce cargo load and it is beneficial to use turbopump instead. [18, 45]

The main thrust rocket engines with electrically pumped propellant at the time of writing are the Rutherford engine with a thrust of 22 kilonewtons and the Delphin engine with a thrust of 28 kilonewtons. These engines are used in rockets designed to take satellites of up to 100 kilograms to low earth orbit. [45, 9]

Chapter 4

Cavitation

Cavitation is a physical phenomenon characterized by the formation of a region of very fine bubbles of liquid that have evaporated at normal temperature. This phenomenon is usually undesirable as it compromises the function and reduces the service life of hydraulic machinery.

4.1 Physical essence

Cavitation can be well visualized on a phase diagram. It shows that the state in which a substance occurs is a function of temperature and static pressure. If the static pressure drops, the fluid can change to a gaseous state without the need to raise the temperature. Instead, the temperature of the liquid drops because thermal energy is consumed in the phase transformation. In hydraulic machines, regions of low static pressure are common, which can be deduced from the law of conservation of mechanical energy, see (4.1). In general, in regions of high flow velocity, the value of static pressure decreases. For example, this manifests itself in confusor. At the same time, the pressure decreases with geodetic height, so there may be a risk of cavitation developing in the delivery pipes. At the same time, the law of conservation of momentum shows that the static pressure drops when the fluid flow curves significantly, which is a risk in rotating hydraulic machines. [30]

$$\frac{p}{\rho} + \frac{v^2}{2} + gh = constant \tag{4.1}$$

where p is the pressure, ρ is the density of the fluid, v is the velocity of the fluid, g is the acceleration due to gravity, and h is the height of the fluid above a reference point.

In order for cavitation to develop, saturated vapor pressure needs to be achieved in the flowing fluid. However, once cavitation begins, the heat of the liquid is converted to latent heat required for phase change. Because of this, the liquid will decrease its temperature. This cooler liquid will eventually re-enter the high-pressure region where the cavitation bubbles will again condense and the liquid temperature will return to its original level. However, since the saturation vapor pressure value decreases with decreasing temperature, cavitation is at least slightly automatically suppressed.

The bubbles developed in the low-pressure regions are then entrained by the flow into regions where the pressure increases again and the contents of the bubbles condense

into a liquid. Bubble collapse is a very fast phenomenon and is strongly influenced by the surrounding geometry. As a result of the limited flow near the wall, the bubbles collapse asymmetrically to form a toroid. A highly accelerated liquid then flows through its center. The direction of this jet is oriented towards the container wall and exerts significant stress on the surface of the equipment. Since this phenomenon is repeated thousands of times per second, it is the main cause of cavitation erosion, which reduces the lifetime of the device.

However, for the needs of a rocket engine pump, cavitation is much more significant in terms of disrupting the flow path and interrupting pump operation. If too large a cavitation region develops, the pump can become clogged. In contrast, a minor cavitation occurrence is not problematic because the pump's planned operating life is not long enough to experience cavitation erosion.

In addition to temperature and pressure, the development of cavitation is also influenced by other properties of the fluid.

The size of the surface tension of the phase interface has a significant influence on the development of cavitation bubbles. Higher values of surface tension slow down the growth of cavitation bubbles but contribute to the rate of their collapse. [30]

Another factor strongly influencing the development of cavitation is the purity of the fluid. Contamination by suspended solids or gases provides favorable conditions for phase transformation and nucleation of cavitation bubbles. By reducing the required activation energy for phase transformation, the pressure at which cavitation is likely to occur is effectively increased. In this case, the type of phase interfaces strongly matters. If the strength of the interphase interface is higher than the strength of the liquid molecules, the interface is not a nucleation site for cavitation bubbles. [30]

At the same time, the viscosity of the liquid is assumed to stabilize the formation and disappearance of cavitation bubbles. However, this assumption is difficult to measure because higher viscosity flows achieve higher pressure decrease due to viscous energy dissipation around the bubbles.

4.2 Cavitation in centrifugal pumps

This chapter will discuss the behavior and characteristics of pumps affected by cavitation presence. Cavitation is problematic for pumps because, it occurs in the low-pressure region, i.e. at the suction. Its effects then propagate through the equipment and affect its performance throughout its entire volume. This differentiates pump cavitation from pressure turbine cavitation, where cavitation develops at the outlet of the impeller and is quickly removed from the turbine.

4.2.1 Suction specific energy

Pump behavior during operation with the presence of cavitation must be quantitatively determined for use in engineering practice. For this purpose, a series of tests have been

developed to which the pumps are subjected. Based on the results of these tests, so-called suction-specific energy is derived, which is then used to compare the different pump types. [15]

Due to the complexity of the problem, several parameters based on a modification of the specific suction energy formula have been established 5.1.4. The individual parameters describe the effect of cavitation on a specific pump attribute and its function in different conditions.

Outer characteristics

The external pump characteristics include those qualities that are useful when designing systems containing pumps. They usually describe the conditions that need to be met in order for the pump to operate reliably.

The fundamental external characteristic of the pump is the suction-specific energy. Its relationship is defined in the equation 4.2 and is measured experimentally. [15]

$$Y_s = \frac{p_{abs} - p_{bar}}{\rho} + g \cdot y_s \tag{4.2}$$

There are two pressure values in the formula. First, the barometric ambient pressure and second, the absolute pressure inside the lower tank. The experiment proceeds by monitoring the pump performance and reducing the pump suction pressure in steps. This can be done either by lowering the closed loop pressure with a vacuum pump, by changing the pump position, or by changing the water level in the bottom tank. During this pressure drop, the decrease in the specific energy transferred to the fluid is monitored and the minimum operating pressure at the pump inlet is determined. This value is further converted to critical suction-specific energy, which is further adjusted to the allowable suction-specific energy. These values can be further converted to other parameters 5.1.4.

Inner characteristics

In contrast, the parameters describing the internal characteristics of the pump are important in the pump design. The main representative of these parameters is the so-called cavitation depression. This is again a variable based on the specific energy of the fluid, but this time expressed as a function of parameters that are relevant to the designer of the device itself.

$$\Delta y_{krit} = \frac{p_{s1} - p_{sat}}{\rho} + \frac{c_1^2}{2} \tag{4.3}$$

The cavitation depression is defined by the formula 4.3, and involves parameters that are chosen by the pump designer. Those being the static pressure and the liquid velocity at the pump inlet. There are, however, fluid parameters that constrain the designer and cannot be influenced. These are the density of the liquid and the saturation vapor pressure. [15]

4.2.2 Tip cavitation

As shown in Figure 4.1, the blades of the finite length are bypassed via the tip gap due to the pressure difference between the suction and pressure sides. This is an unfavorable phenomenon that reduces the characteristics of the machine. The tip gap introduces additional volumetric losses into the machine and a tip vortex is formed near the gap, which dissipates the fluid energy. This low pressure vortex further enhances the bypass effect. The low pressure in the core of the vortex can serve as a cavitation nucleation region. In addition, this vortex affects the practical hydraulic shape of the blade by preventing the free flow of the fluid. [15]

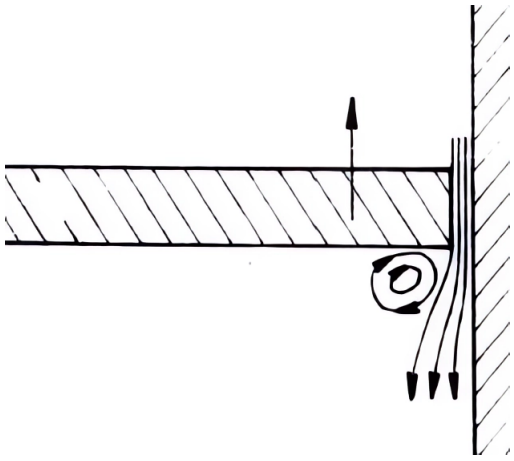

Figure 4.1: Blade tip cavitation [**?**]

Tip cavitation is mainly influenced by the clearance between the blade tip and the shroud. It is beneficial to select the smallest possible gap size tolerance the manufacturing technology allows.

4.2.3 Leading edge cavitation

The most important location of cavitation in centrifugal pumps is the inlet. This is the high velocity region at which the pump has not yet been able to provide any specific energy to the fluid. The leading edges of the blades are then particularly problematic. The moment a blade is inserted into the flow path, the area is reduced and the velocity must necessarily increase, which, based on the conservation of energy law (4.1), reduces the static pressure of the flowing fluid. In addition, the blade forces the fluid to change direction, which affects the pressure field distribution. [15]

The leading edge of centrifugal pump blades is not shockless and requires the presence of an incidence angle or blade angle of attack for proper operation. This is the angle between the fluid velocity vector and the blade leading edge angle. For axial stage pumps, an incidence angle between 1 and 4 degrees is commonly used. This angle forces the fluid to change direction immediately after contact with the blade. However, this has the disadvantage of creating a low pressure region on the suction side of the blade. The pressure

in this area can drop below the saturation vapour pressure of the fluid, and cavitation can occur.

Depending on the operating clearance, the meridional velocity of the inlet fluid varies and so does the angle of incidence. This is particularly critical when the flow rate is reduced, as the angle may disappear completely or even become negative. In this case, the pump impeller would draw specific energy from the liquid and the liquid would lose pressure in the beginning of the impeller channel. The pump would then be at risk of being blocked by cavitation and completely stalling.

4.3 Effects of cavitation

The characteristics of the behavior of hydraulic machines can be greatly impacted by cavitation. The presence of a cavitation region can reduce operating parameters such as head, efficiency, and flow rate. However, cavitation can also impact long-term pump function by introducing vibrations and erosion of the equipment.

4.3.1 Erosion

In the case of long-term operation of hydrodynamic machines, cavitation is problematic mainly because of the erosion that accompanies it. Fully developed cavitation erodes the material of the equipment, which shortens its service life considerably.

Erosion occurs due to three main mechanisms. The first is the formation of a liquid jet as the bubble collapses. This jet is directed towards the machine wall and significantly increases the surface load, causing plastic deformation of the material. The second phenomenon is the effect of high temperature. This happens as the volume of the cavitation bubble is subjected to substantial compression at collapse, resulting in an increase in the internal temperature of up to tens of thousands of Kelvin. This high temperature transmits to the surface of the machine and degrades its mechanical properties. Finally, the formation of an electrical cell between the wall and the flowing fluid is also involved. Due to the high temperature inside the bubble, chemical reactions take place between the substances contained in it. These substances are often heterogeneous, since it is the external particles mixed in the liquid that often serve as nucleation sites for the formation of bubbles. The resulting compounds can then be electro-chemically charged and react with the wall. [15, 30]

4.3.2 Vibrations

The optimum running of cavitation-free rotary hydrodynamic stators is characterized by the only sound emitted being the friction of seals and bearings and that of a fluid flow. However, when cavitation is present, the noise caused by the pressure shocks generated by collapsing cavitation bubbles is present. The noise manifests itself in the range of 10 Hz - 3 MHz.

The noise is a consequence of the pressure pulsations and therefore there are vibrations propagating through the device along with the noise. The problem with broadband noise is that it manifests itself at all frequencies. The device is therefore in resonance at all natural frequencies simultaneously. The amplitudes of the resulting vibrations can therefore be amplified severalfold and can threaten the life of the bearings, but also the impeller itself in terms of fatigue life. [15]

Chapter 5

Centrifugal pumps

The centrifugal pump utilizes the principle of centrifugal force to convert driver energy to kinetic energy of the pumped fluid. It consists of a rotating impeller spinning inside a stationary casing. Impeller has a geometry designed in such a way that generates a low-pressure zone at the center, which draws fluid into the pump. Propeller blades then propel the fluid outwards, which increases the fluid velocity and pressure. [21]

Centrifugal pumps have the ability to be designed for a wide range of volume flow and pressure gain as well as a wide range of pumped fluids. Their only moving part is the spinning impeller, which requires no valves for its function. Therefore they do not require complex maintenance. Compared to other types of pumps, they are also highly efficient at up to 93 percent. [36]

5.1 Characteristics

The pump characteristics describe the behavior of the pump in a certain sense that is useful for the design of the pumping system. They are often measured in the laboratory or based on CFD results. They are often presented as a function of flow at a specified speed and can be calculated for different speeds based on hydraulic similarity or can be defined over the entire operating range.

5.1.1 Head

The head is the measurement of the kinetic energy created in a pump. It measures the height of the liquid column the pump could create based on the kinetic energy transferred to the fluid. It is generally defined by impeller speed and diameter. The benefit of using head instead of pressure gain to describe pump performance is that the pressure gain is dependent on fluid density, whereas the head is constant. [21]

5.1.2 Efficiency

Pump efficiency is defined by the ratio of the energy transmitted to the fluid to the energy consumed by the pump. For centrifugal pumps the usual range for efficiency is thirty to

ninety percent. The lower efficiencies are due to energy losses, which can be caused by mechanical and hydraulic friction, leakages induced by pressure differentials within the pump case, and by operation outside of optimal parameters such as the impeller blade angles not matching the fluid movement and large swirling and recilculation are induced. [21]

Efficiency is often considered mainly to conserve energy and cost. However it can also be important, as the pump with higher efficiency requires a less powerful motor and less shaft torque to operate, which can lower motor cost and weight.

5.1.3 Rotating stall

Centrifugal pump rotating stall is a condition where the pump fails to deliver flow rate and head based on characteristics. This is usually caused when the flow rate at a set speed is reduced below a certain point. The mechanism of the rotating stall is caused by fluid separation from the impeller blades and forming of low-pressure pockets. In these pockets, cavitation can develop. This causes a sudden drop in flow rate and pressure, and can damage the hydraulic system. [21, 27]

It can generally be said that the stall occurs when the angle of incidence nears zero. When this happens, the suction side of the pump begins consuming fluid energy, hence lowering its pressure. This is mainly problematic in axial pumps, which are very sensitive to blade angles.

5.1.4 Net positive suction head

The low-pressure region in the center of a pump presents a risk of cavitation development.

Net positive suction head or NPSH is a function indicating the value of the pump suction pressure required for its safe operation without significant cavitation. It is equivalent to cavitation depression but is represented as fluid column height. The relation between these two parameters is shown in (5.1)

$$NPSH_R = \frac{\Delta y_{krit}}{g} \tag{5.1}$$

Where „R“ stands for „Required“. For this thesis however the parameter $NPSH_3$ will be used. It is defined as the suction head at which the pump-specific energy gain reduces by 3 percent.

The NPSH value can be affected by the liquid temperature and the geometric layout of the cavitation regions. Together with the heat consumed for phase transformation, the lower temperature of the drawn-in fluid may reduce the NPSH. This behavior is included in the Thermodynamic Suppression Head (TSH) term and can be approximated using empirical formulas. This term is then added to $NPSH_A$

5.2 Force

Centrifugal pumps do not have any parts in translational motion, so there is no need to capture the inertial forces of these parts. Despite this, however, significant loads can be exerted on the pump impeller either by gravity or by the pressure of the pumped fluid. The forces are also essential in determining the required impeller clearances because they bend and stretch the impeller shaft. As bearing life design is based on these loading forces, models have been created to approximate these loads.

5.2.1 Axial force

The axial force acting on the pump impeller is caused by the curving of the fluid flow direction and the pressure field asymmetry caused by the pump inlet area.

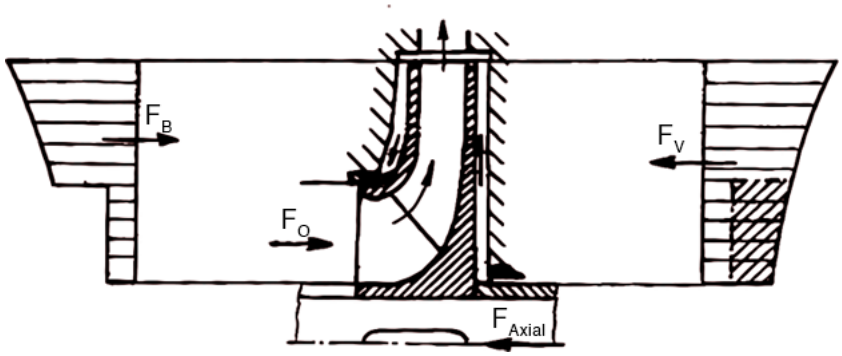

Figure 5.1: Pressure distribution causing axial force [21]

The pressure values acting on the axial projection surfaces are important for the axial force. It can be assumed that the pressure inside the impeller nozzle is the same at both the hub and casing and cancels out. A circumferential fluid velocity equal to half the impeller velocity is assumed for the determination of the pressure in the sealing gaps. The pressure is then determined on the basis of centrifugal acceleration and momentum conservation law. The impeller inlet area is assumed to be at the pressure of the intake manifold. As can be seen in Figure 5.1 these forces are not in equilibrium and the axial force can be determined by the formula (5.2) This relationship makes use of other simplifications of the geometry, such as not including the pressure acting on the impeller mounting nut, or assuming an idealized pressure drop in the seal rings.

$$F_{ax} = \pi\rho \left[\frac{p_2 - p_1}{\rho} \cdot (r_T^2 - r_n^2) - \frac{\omega^2 R_2^2}{4} \cdot \frac{r_T^2 - r_n^2}{2} + \frac{\omega^2}{4} \cdot \frac{r_T^4 - r_n^4}{4} - v_{m0}^2 (r_T^2 - r_n^2) \right] \quad (5.2)$$

where F_{ax} is the axial force acting on the impeller, p_1 is stage inlet pressure, p_2 is stage outlet pressure, ρ densinty of the pumped fluid, r_T is impeller inlet radius, r_n shaft radius, R_2 is impeller outlet diameter, ω is impeller speed, and v_{m0} is inlet axial velocity of the fluid.

There are several pump design modifications that can be applied to reduce the axial force. Most commonly, the axial force is compensated by drilling through holes connecting the back disc seal gap and the impeller vane. Another option is to install a double-sided impeller or to install two pumps with opposite orientations. For rocket engines, it is possible to install impellers for the fuel pump and the oxidizer pump on the same shaft. Other common methods of axial force reduction include adjusting the sealing ring position and impeller shaft diameter. The sealing ring behind the impeller may be installed at a diameter such as to compensate for the pressure acting on the impeller inlet area.[39]

5.2.2 Radial force

The radial force acting on the impeller is caused by an asymmetrical geometry. It can be caused by an asymmetrical velocity field of the incoming fluid, which can be induced, for example, by an elbow upstream of the pump. But the main component of the radial force is induced by an asymmetrical pressure distribution on the pump spiral entrance, which is usually caused by its tongue. This force can often be eliminated by inserting a vane into the pump volute. This vane has the same geometry and is mounted symmetrically against the tongue of the volute so that their pressure distributions balance each other. [14, 21]

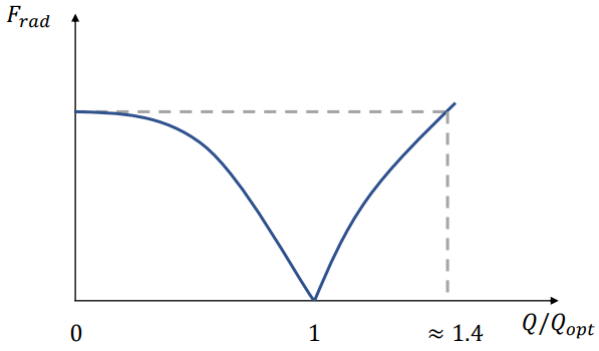

Figure 5.2: Radial force magnitude as a function of flow rate according to Biheller [14]

As can be seen in Figure 5.2, the radial force is evident mainly during an operation outside the optimum flow, and the Biheller procedure is used to determine it. This is based in part on empirical formulas and recommendations for spiral design. For a classical spiral and impeller, the relationship (5.3) can be applied.

$$F_{rad} = 0.221 \cdot u_2^2 \cdot S \cdot \rho \cdot 10^{-1.13 \cdot \frac{A_n}{A_{vsd}}} \cdot \sqrt{1 + (\frac{Q}{Q_{opt}}) - 2 \cdot \frac{Q}{Q_{opt}} \cdot cos\beta_2} \tag{5.3}$$

where F_{rad} is the radial force acting on the impeller, u_2 is the impeller outlet circumferential speed, ρ is fluid density, A_n is the area causing the radial force, A_{vsd} is the spiral outlet area, Q is the current flow rate, Q_{opt} is the optimal flow rate, and β_2 it the blade's trailing edge angle.

The problem with this force is its periodic nature during rotor-stator interaction at each pass of the blade. This force therefore cyclically stresses the pump shaft, which should be checked for fatigue life and eventually resonance.

Chapter 6

Materials

Pump components can also be coated with metallic, non-metallic, and ceramic compounds in order to increase resistance to corrosion and wear. These coatings can also be used to repair damaged and worn components.

Chemical compatibility of components and pumped medium is normally provided by pump manufacturers. It is important to consider this factor when designing a new pump as an unwise combination of materials in the loop can severely increase corrosion and in the case of plastics can cause softening and swelling. This can vary based on the concentration, temperature, or presence of abrasives in a pumped medium. In some cases, it is necessary to carry out tests under field conditions to verify the longevity of the machine's operation. [11]

6.1 Cast iron

Cast iron can generally be described as a ferrous alloy containing silicon and more than 3 percent of carbon. This carbon then precipitates into graphite. This alloy has a low melting temperature and low viscosity. Therefore, it is cheap to cast into complex shapes in one piece. Graphitic cast iron is easy to machine, has good corrosion resistance to neutral and alkaline liquids and has roughly 7 percent lower density compared to steel. It, however, also weakens the alloy's mechanical properties and makes it impossible to weld and repair portions containing a crack or cavitation damage.

6.1.1 Gray cast iron

Gray cast iron forms directly by crystallization from the liquid. Graphite has a lamellar structure and is encased in ferit or perlitic matrix. The lamellar shape of graphite generates areas of large stress concentration at the lamella tips. It is therefore very brittle and its ultimate tensile strength doesn't exceed 450 MPa. Its compressive strength can however reach 1200 MPa. Graphite precipitates are held loosely in the matrix and provide strong vibration-dampening. [3]

Because of that, grey cast iron is being used in pump design mainly to create housings and holders, where vibration-dampening characteristics are beneficial and no shocks are to be expected. However, it must not be used on pump casings where safety is an issue.

6.1.2 Nodular cast iron

By following the graphitization procedure, which consists mainly of slow cooling and staying at a specific temperature for a particular time, lamellar graphite can turn spherical. Cast iron with spherical graphite can often be compared to steel in mechanical properties. Spherical graphite grains do not produce strong stress concentration regions and do not support crack formation. Therefore the material is ductile and not prone to brittle fracture. This material can reach yield tensile strength of 600 MPa and ultimate tensile strength of 900 MPa. [3]

Nodular cast iron has lower hardness and erosion resistance than gray cast iron. Austenitic cast iron containing fifteen to twenty percent of nickel can be used for manufacturing impellers for seawater pumps.

6.2 Steel

Alloys of iron and carbon without graphite content are called steels. Their properties vary significantly depending on alloying elements and the heat treatment process. It can be machined, cast, and sometimes welded. Cast steel impellers can be used to pump liquid at temperatures above 150°C.

6.2.1 Carbon steel

The cheapest type of steel is common carbon steel. It does not form a protective surface layer and is therefore susceptible to corrosion. It can only be used in combination with mediums not containing oxygen. It has low mechanical properties and is not commonly used in impeller design. [8]

6.2.2 Stainless steel

Stainless steel contains at least 15 percent of chromium, which forms an inert oxide surface layer. This binds to the surface and protects the underlying metal in highly corrosive environments. Stainless steel usually also contains a significant amount of elements such as nickel, molybdenum, and manganese. Based on the distribution of its elements, the stainless steel alloy can be differentiated into four groups, each of which has its specific crystal structure: austenitic, ferritic, martensitic, and duplex. [3]

The most commonly used types of stainless steel in pump design are austenitic 300 series. The most frequently used AISI 304 grade contains 18 percent chromium and 8-10 percent nickel. Another, also frequently used type, is AISI 316 grade, which also includes 2 percent molybdenum, and has greater resistance to acidic corrosion. Austenitic steel is usually very ductile and both of these can reach yield tensile strength of 280 MPa and ultimate tensile strength of 500 MPa while maintaining high hardness and both mechanical and cavitation resistance. [7, 3, 11]

Duplex-grade stainless steel is a branch of two-phase austenitic-ferritic in roughly equal proportions. They are designed to provide better corrosion resistance and higher strength.

They have higher chromium content (20-28 percent), higher molybdenum (5 percent), and lower nickel (9 percent). Higher strength enables thinner walls, which improves hydraulic efficiency while also lowering manufacturing costs. For example, UNS S32202 stainless steel can reach a yield tensile strength of 510 MPa and ultimate tensile strength of 740 MPa. [7, 33, 3]

Martensitic steel contains less than 5 percent nickel and, when quenched properly, can have a high ultimate tensile strength of up to 1200 MPa. It is however prone to local corrosion and its use is limited to mildly corrosive mediums, such as freshwater or demineralized water. One of the most commonly used materials for highly loaded impellers is martensitic steel EN 1.4317, because of its high strength and cavitation resistance. [7, 3]

6.3 Aluminium

Aluminum is material with low density at roughly one-third of the density of steel. The alloy commonly used for impeller design is EN AL 6061. This alloy is thermally treated for yield tensile strength of 270 MPa. It has strong corrosion resistance against acidic mediums, but is very sensitive to alkalic mediums and has low cavitation resistance. [13]

6.4 Copper

Copper alloys are usually called bronzes and can vary depending on the alloy element. However, the most common copper alloy for impellers is brass, which is an alloy of copper and zinc. Reliably pumping corrosion-causing liquids with salt content can be achieved by using a brass impeller. It has high resistance to corrosion and cavitation erosion, while having an ultimate tensile strength of up to 650 MPa. It also has the ability to dry run. It is commonly utilized for power generation, seawater, and oil pumping. [4, 13]

6.5 Superalloys

Nickel-based „superalloys“ are materials suited for operation in extreme environments. They have very high corrosion resistance and are able to be deployed in high temperatures. They are generally known by their trade names, the most common being INCONEL® 718.

INCONEL® 718 consists of 50-55 percent nickel, 17-21 percent chromium, 2.8-3.3 percent molybdenum, 4.75-5.5 percent nobelium and tantalum, 1 percent cobalt, and 0.65-1.15 percent titanium. Other elements include iron, copper, manganese, aluminum, silicon, carbon, sulfur, phosphorus, and boron. [6] Its mechanical properties can be found in the Table 6.1.

Table 6.1: Important design properties of Inconel 718 alloy

Density	8190	$kg{\cdot}m^{-3}$
Yield strength	1030	MPa
Ultimate strength	1240	MPa
Hardness	335±9	$HV0.5$
Minimum temperature	-253	$°C$
Maximum temperature	704	$°C$

6.6 Plastic

The most common plastic type used for pump impeller design is thermoplastic. This is a type of plastic resistant to most liquids that corrode metals. Its main characteristic is the ability to be softened by heating and molded or cast into complex shapes. Their mechanical properties can be reinforced with fillers such as glass fiber. But its mechanical properties are still inferior to metals. [11]

Many pump components are being manufactured out of PTFE (Teflon®), which has great corrosion resistance and chemical inertness. It also has a wide operating temperature range of up to 250 $°C$.

Chapter 7

Concept design

The first step in the design of any device is to determine exactly what properties are desired. In this case, it is a rocket engine oxidizer pump. The goal of this device is to minimize the necessary suction line pressure when compared to a purely radial impeller, while also achieving the desired flow rate and pressure gain.

The impeller, however, is not the only component of the pump. The pump consists of an electronic section, a mechanical section, and a hydraulic section. The whole scope of this thesis will deal only with the hydraulic portion that is to be integrated into the pump. It is, therefore, necessary to consider its integration into the whole system and to ensure its compatibility with the other components of the machine.

7.1 Motor

The reason why electrically driven rocket engine fuel pumps are even being considered is because of developments in electronic technology. In particular, battery technology has a higher energy density than it had in the past. Thus, it is now becoming economically viable to fit electrically driven pumps instead of gas-powered turbopumps into small rocket engines.

Because of the reduction in equipment weight, there is an effort to maximize the power density of the electric motor. This is done primarily by increasing its speed. Assuming a sufficiently efficient dissipation of waste heat, a maximum power density of about 7 kilowatts per kilogram is currently achievable.

The whole pump concept revolves primarily around the proposed motor. The motor used for the pump designed within this thesis will operate at a mechanical power of approximately 3500 watts at 70 000 revolutions per minute.

7.2 Inducer

It is necessary to decide whether it makes sense to incorporate the inducer into the pump at all. The inducer is a lower-efficiency pump that also has a narrower operating flow win-

dow. Therefore, its implementation only makes sense if the purely radial stage is unable to operate at the required inlet line pressure as described in chapter 5.1.4. [34]

If an inducer is required, the question is whether to try to incorporate it into the impeller of the radial stage or to develop a separate axial stage impeller upstream. The combination of axial and radial stages may have advantages and disadvantages over a separate configuration. The main issue limiting this solution is the complexity of the blade curvature. Since properly designed inducer blades have a backsweep that twists them extensively, this geometry must transition freely into the blade shape required for the radial stage. The resulting impeller may then be less efficient than two separate stages of optimal geometry. However, a loss caused by the shock at the radial stage blade's leading edge and recirculation loss at the inducer trailing edge are eliminated, which can improve pump efficiency.

Since the version of the impeller with an incorporated inducer is not as common, one of the main goals of this thesis is to assess its performance.

7.3 Cover disc

The implementation of the cover disk is mainly influenced by manufacturing technology. In general, from a hydraulic point of view, it is always preferable to have the impeller fitted with a cover disc. Covered impellers achieve higher efficiency due to smoother channel geometry and are at no risk to volumetric losses and the induced vortex shedding at the blade tip, nor the development of tip cavitation.

Impellers for conventional centrifugal pumps are usually cast or milled. However, the impeller proposed in this thesis will have a diameter of a few centimeters, with blades several millimeters high and approximately a millimeter thick. These dimensions are unattainable for castings. The usual approach would therefore be to mill them. However, this does not allow the implementation of a cover disc, as the tool would not be able to reach the channels. A third option is offered, which is the SLS 3D metal printing method. This technology can produce the impeller including the cover disc. However, the parts produced by this technology fall short of the surface quality required for conventional hydraulic machines.

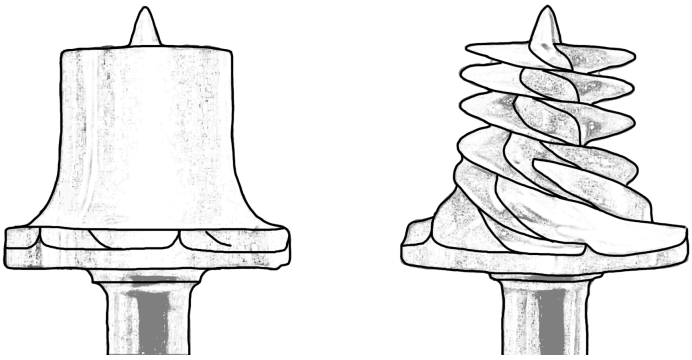

Figure 7.1: Comparison of high-speed pump impellers with and without cover disc [1]

It is therefore important to decide which approach is the most advantageous for this pump; whether the pump impeller will be manufactured without a cover disc with a high-quality flow channel surface, or whether the impeller will be covered but will have a rough surface. One of the designs will be chosen based on the results of CFD simulations of both open and covered impeller designs. The axial stage is expected to be very sensitive to surface roughness, while the radial stage should be able to handle a poorer-quality flow path. It is therefore also possible to only use cover the radial stage.

Chapter 8

Radial stage design

For the first iteration of the design, a purely radial centrifugal pump was chosen to provide the entire pressure gain. This pump uses a simple design that contains no moving check valves, and is, therefore, very reliable. It can be expected that a purely radial design will not be able to operate at the required inlet pressure without the presence of a significant cavitation region. Because of this, the results of this design will be used as input to the following design of the axial pressure booster pump upstream of the radial pump.

8.1 Target parameters

The proposed oxidizer pump should achieve the parameters shown in the following Table8.1. The pump should also be designed to be capable of long-term operation in terms of mechanical stress and erosion. Considering either the impeller or the entire pump assembly, the design should be able to withstand operational vibrations.

Table 8.1: Target parameters for radial stage design

Rotating speed	70000	rpm
Hydrogen peroxide	87-98%	H_2O_2
Density	1400	$kg \cdot m^{-3}$
Dynamic viscosity	0.00125	$Pa \cdot s$
Vapour pressure at 20°C	216	Pa
Mass flow rate	1.3	$kg \cdot s^{-1}$
Pressure gain	28	bar
Suction pressure	2	bar

$$H = \frac{\Delta p}{\rho \cdot g} = 203.9\, m \tag{8.1}$$

A pump with these parameters of the conveyed medium has a delivery head of 203.9 meters (see 8.1) and is described by a specific speed of 144.8 rpm (see 8.2).

$$n_s = 3.65 \cdot \frac{n \cdot \sqrt{Q}}{\sqrt[4]{H^3}} = 144.3\, min^{-1} \tag{8.2}$$

8.2 Analytic design

The hydraulic design of a centrifugal pump is based on the combination of principles of potential flow and sets of empirical corrections of real designs, from which preliminary equations are derived to determine the pump parameters. These equations can be inverted, and, in turn, used to determine the pump impeller dimensions based on the required parameters.

The determination of the impeller outlet diameter is based on the Euler pump equation modified for rotating machines (8.3), which factors in the required pump pressure gain. This can be further modified into a quadratic equation, the solution of which allows us to obtain the value of the output circumferential velocity required for the desired pressure gain.[21]

$$\frac{g \cdot H}{\eta_h} = \kappa \cdot u_2^2 - \frac{v_{m2}}{tan\beta_2} \cdot u_2 \tag{8.3}$$

The pressure gain is then approximately quadratically dependent on the impeller outlet circumferential velocity (8.4). It then depends on the rotational speed of the impeller and its diameter. Since the pump is driven by a 70000 rpm electric motor, circumferential velocity can be determined and further used to obtain the pump impeller diameter. The number of impeller blades and their trailing edge angle is included in the formula using the slip factor correction κ (8.5), according to Waisser.[21]

$$u_2 = \pi \cdot D_2 \cdot n \tag{8.4}$$

$$\kappa = 1.01 - \frac{0.395 + 0.457 \cdot sin\beta_2}{\sqrt{z}} \tag{8.5}$$

The outlet width b_2 of the pump impeller is the dimension affecting the velocity of the liquid leaving the pump and consequently the flow rate. Its appropriate choice depends on several factors according to equation (8.6). One of them is the blade trailing edge angle β_2, which is usually in the range of 20-35 degrees. This angle influences the stability of the pump $Q - H$ characteristic.[21]

$$b_2 = \frac{Q}{v_{m2} \cdot (\pi \cdot D_2 - \frac{z \cdot \Delta}{sin\beta_2 \cdot cos\gamma_2})} \tag{8.6}$$

The impeller inlet diameter is determined by empirical formulas derived by measuring a large number of different impeller designs. Figure 8.1 shows that it is appropriate to choose the impeller inlet diameter as a function of the outlet diameter and the specific speed. The specific speed of the desired pump is 144.3 rpm. For this specific speed, pumps with a suction diameter equal to roughly 50 percent of the impeller outlet diameter achieve the highest possible efficiency. Impeller axial extend can be determined using similar empirical formulas based on specific speeds. In this case, the recommended axial width is 20 percent of the outlet diameter.[21]

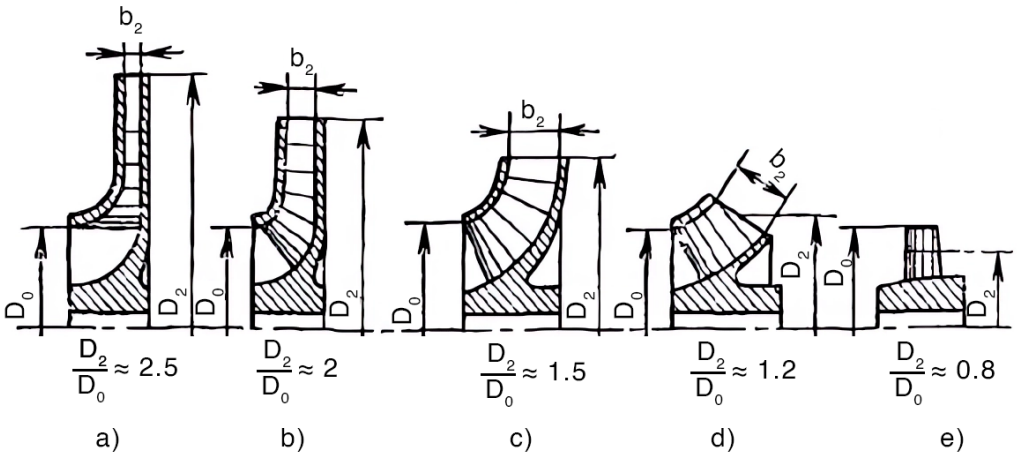

Figure 8.1: Comparison of radial impeller designs based on its specific speed: a) - low specific speed impeller $n_s = 40 - 80$, b) - standard specific speed impeller $n_s = 80 - 150$, c) - high specific speed impeller $n_s = 150 - 300$, d) - diagonal impeller $n_s = 300 - 600$, e) - axial impeller $n_s = 600 - 1200$ [16]

Alternatively, it is possible to design an impeller inlet area based on the blade leading edge meridional velocity. This can be approximated as a function of the pump delivery head with a correction for the given geometry k_{m1} based on the assumption of mechanical energy transformation. For a specific speed of 144.3, it is defined as:

$$k_{m1} = 0.12 + 0.5617 \cdot (8.2372323 \cdot 10^{-4} \cdot n_s - 0.041)^{0.8} \tag{8.7}$$

$$v_{m1} = k_{m1}\sqrt{2 \cdot g \cdot H} \tag{8.8}$$

The meridional velocity at the pump inlet (8.9) can be assumed to be 10-20 percent lower than at the leading edge of the vane. The continuity equation can then be used to determine the pump inlet diameter (8.10) needed to achieve the desired liquid inlet velocity.[21]

$$v_{m0} = (0.8 - 0.9) \cdot v_{m1} \tag{8.9}$$

$$D_0 = \sqrt{d_0^2 + \frac{4 \cdot Q}{\pi \cdot \eta_V \cdot v_{m0}}} \tag{8.10}$$

The axial width (8.11) of the impeller is then determined as a function of the pump inlet diameter and the specific speed.

$$z_E = 0.75 \cdot \frac{D_0 - d_0}{2} \cdot n_s^{-0.05} \tag{8.11}$$

The angle of attack of the blade β_1 can be determined from the velocity triangle at the pump inlet. A blade angled in this way will result in a shock-free flow of fluid. However, the blade area blocks the flow and increases the meridional velocity. Such a blade would then be too angled, resulting in the front section of the blade acting as a turbine and in turn reducing the pressure in the fluid. This problem is solved by assuming an incidence angle at the leading edge of the blade (see equation (8.12)). The resulting angle of attack is then defined by the incidence angle. The smaller this angle is, the smaller the low-pressure area on the suction side of the blade, and the pump is able to operate at a lower inlet pressure. Such a pump is however more susceptible to flow drops. The angle of incidence is normally chosen based on the experience of the designer but is generally recommended in the range of 2-4 degrees.[21]

$$\beta_1 = arctan\frac{v_{m1}}{u_1} + i \tag{8.12}$$

The angle of the leading edge is different than the angle of the trailing edge of the blade. It is therefore necessary to curve the blade to match both angles. There are two primary approaches to blade curvature. The first is a linear change in angle, which is characterized by the minimum possible blade length and the lowest viscous losses. The disadvantages of this method are that there are not enough degrees of freedom in the design and that the blade then has a predefined wrap angle. Both sides of the blade have the same wrap angle, which for radial impellers results in increasing blade thickness with radius. The method with a quadratic change of blade angle is significantly more advantageous in design. This method has one more degree of freedom and allows for control of the wrap angle and associated blade thickness.

In an attempt to minimize the required suction pressure and pressure pulsations caused by the interaction of the spiral tongue with the impeller blades, it is advisable to divide the blades into several curves along the width of the blade and have both the leading and trailing edge of the blade slanted. However, even a quadratic change in blade angle is only applicable to simpler impeller geometries for manufacturing reasons. Instead of a polynomial angle change function, it is possible to use Bezier curves, which define the angle of rotation along the entire length of the blade based on a small number of control points. This can ensure the manufacturability of the impeller.

8.3 Design features

The design of a centrifugal pump involves the creation of a complex geometry describing the shape of the blade, which is usually handled in the form of strongly curved mathematical curves. The theoretically optimal blade geometry is often not manufacturable using available manufacturing methods. The main problem appears to be in the slope of the blades, which does not allow cutter access. Therefore, efforts are made to limit this slope in some way. At the same time, the objective is to minimize the restriction of the flow passage by the blade area, which reduces the tendency of the pump to develop cavitation.

8.3.1 Slanted outlet

The blade is a complex geometry and due to the differences between the leading edge angle and the trailing edge angle, it is necessary for the blade to be curved. Even more so when the impeller has an axial inlet and the leading edge angle changes with radius because of different circumferential velocities. This curvature however increases the length of the blade, thereby increasing the viscous frictional losses. Therefore, an attempt is made to minimize the deflection of the blade while maintaining its thickness. At the same time, the shape of the blade needs to be obtainable using available manufacturing methods. It is therefore advantageous to slope the trailing edge of the blade to reduce its deflection. In general, the maximum angle of inclination of a gamma trailing edge blade is recognized to be 20 degrees, which is limited by manufacturing.[21]

The inclined trailing edge of the blade also flattens the radial force pulsations caused by the interaction of the spiral tongue and the individual blades.

8.3.2 Splitter blades

A conventional centrifugal pump has a set of blades that extend the entire length of the meridional section. The choice of a number of blades depends on the desired pump flow rate, the required pressure gain, and the cavitation characteristics of the pump. More blades can to some extent increase the efficiency of the pump as they reduce the development of secondary vortices in the impeller and reduce the slip factor. However, this is only true up to a certain point, where the effect of viscous forces over a larger blade area becomes apparent, and the pump efficiency starts to decline. Pumps with a higher number of blades are able to achieve higher pressure increases as each blade is only able to transfer a given amount of specific energy before the pressure on the suction side drops below the saturation vapor pressure of the liquid, the liquid begins to cavitate, and the flow stalls. The larger number of vanes also stabilizes the pump operation and reduces the radial force pulsations generated by the interaction of the impeller vanes and the volute tongue while also reducing noise.[21]

However, a higher number of blades reduces the flow area at the impeller inlet, where the meridional flow velocity must therefore be increased, increasing frictional losses and static pressure. The impeller inlet is the area most susceptible to cavitation formation and therefore flow obstructions need to be reduced to a minimum. In some cases, it is ideal to utilize splitter blades embedded in the impeller. The leading edge of these blades is

situated in a region where the static pressure is high enough and the flow velocity is low enough that cavitation is not a concern. Thus, at the critical point at the impeller inlet, there are only a small number of blades that span the entire impeller.[21]

8.4 Design specification

The resulting design is a relatively conventional radial impeller, whose main special feature is its miniature dimensions, see Table8.2. The leading edge angle of the blade is adapted to achieve a suitable incidence angle over its entire length, while the trailing edge angle of the blade is constant, see Fig 8.2.

Table 8.2: Radial impeller design dimensions

Number of blades	6	
Inlet shroud diameter	12	mm
Inlet hub diameter	4	mm
Outlet diameter	21.6	mm
Outlet channel width	1.66	mm

A value of 32 degrees was chosen for the trailing edge angle of the impeller blades as it provides a good compromise between stability and the delivery head while maintaining the impeller diameter for which the spiral is modeled.

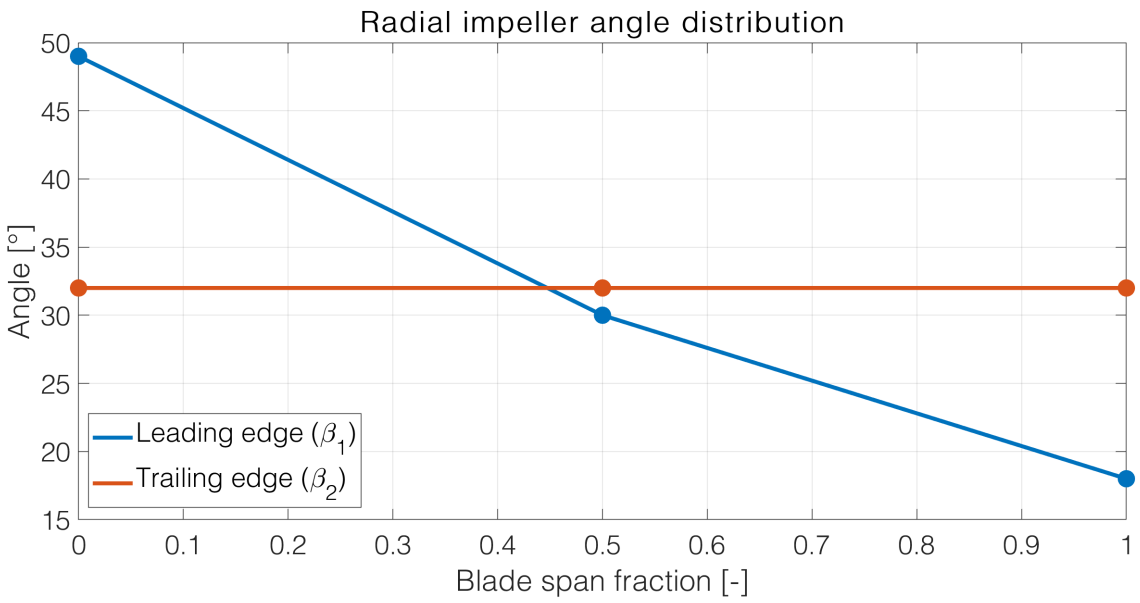

Figure 8.2: Radial impeller blades leading and trailing edge angles

Due to the simplicity of the geometry, only 3 layers could be used to define the blade. Blades have a constant thickness of 0.7 millimeters. This has been agreed upon as possible to manufacture using planned technologies. This value is also very close to what is derived using the formula for the blade thickness of conventional centrifugal pumps. [21]

8.5 CFD simulation

The analytical calculations are based on potential flow assumptions, which are unable to capture the frictional losses in the fluid and the formation of a velocity profile across the impeller vane. They then produce an ideal geometry for the case of non-viscous flow that is not compromised by manufacturing constraints. Therefore, it is common practice to verify the impeller hydraulic design in a numerical computational fluid dynamics environment. [21, 42]

In the case of this study, the software operates based on the principle of the finite volume method. The fluid domain is divided into a finite number of volume elements to which the simplified formulations of fluid mechanics equations are applied. Namely, the conservation of mass in the form of the continuity equation (8.13), the conservation of momentum in the form of Reynolds-Averaged Navier-Stokes equations (8.14), and eventually the conservation of energy equations in the case of non-isothermal problems. [42]

$$\frac{\partial \rho}{\partial t} + \frac{\partial}{\partial x_j}(\rho u_j) = 0, \tag{8.13}$$

where ρ is the density of the fluid, u_j is the velocity component in the j-th direction, and t is time. [43]

$$\frac{\partial}{\partial t}(\rho \overline{u}_i) + \frac{\partial}{\partial x_j}(\rho \overline{u}_i \overline{u}_j) = -\frac{\partial \overline{p}}{\partial x_i} + \frac{\partial}{\partial x_j}\left[\mu\left(\frac{\partial \overline{u}_i}{\partial x_j} + \frac{\partial \overline{u}_j}{\partial x_i}\right) - \frac{2}{3}\mu \frac{\partial \overline{u}_k}{\partial x_k}\delta_{ij}\right] + \frac{\partial}{\partial x_j}(\overline{\tau}_{ij}), \tag{8.14}$$

where ρ is the density of the fluid, $\overline{u}_i$ is the time-averaged velocity component in the i-th direction, $\overline{p}$ is the time-averaged pressure, μ is the dynamic viscosity of the fluid, $\overline{\tau} ij$ is the Reynolds stress tensor (which describes the turbulent fluctuations of the velocity), and δ_{ij} is the Kronecker delta. [43]

The Reynolds Averaged Navier Stokes equations have a significant disadvantage that they cannot correctly evaluate the fluctuation velocity of the flow. They are therefore used in combination with so-called turbulence models, which have been developed from empirical measurements and attempts to approximate the nature of the actual flow. These models are generally divided according to the number of partial differential equations involved in the determination of the fluid fluctuation velocity. [42]

The following partial differential equations describe the $k - \epsilon$ turbulence model that will be used for the CFD simulations. These equations describe the parameters used to model

the simplified turbulent behavior of the fluid. Since accurate turbulence modeling is not essential for the purpose of this thesis, the turbulence model used achieves satisfactory results when validity conditions are met.

$$\frac{\partial(\rho k)}{\partial t} + \frac{\partial}{\partial x_j}(\rho k u_j) = \frac{\partial}{\partial x_j}\left[(\mu + \mu_t)\frac{\partial k}{\partial x_j}\right] - \rho\epsilon \tag{8.15}$$

$$\frac{\partial(\rho\epsilon)}{\partial t} + \frac{\partial}{\partial x_j}(\rho\epsilon u_j) = \frac{\partial}{\partial x_j}\left[(\mu + \mu_t)\frac{\partial \epsilon}{\partial x_j}\right] + C_{\epsilon 1}\frac{\epsilon}{k}\rho\left(C_{\epsilon 3}\overline{} - C_{\epsilon 2}\right) \tag{8.16}$$

where ρ is the density of the fluid, u_j is the velocity component in the j-th direction, t is time, μ is the dynamic viscosity of the fluid, μ_t is the turbulent viscosity (related to k and epsilon), and $C_{\epsilon 1}$, $C_{\epsilon 2}$, and $C_{\epsilon 3}$ are model constants. The terms ϵ and k are the turbulence quantities, where ϵ represents the rate at which turbulent kinetic energy is dissipated by turbulence, and k represents the turbulent kinetic energy itself. [42]

8.5.1 Preprocess

The calculations were performed in Ansys Workbench as it facilitates almost the whole design process of the pump and also features some specialized tools such as BladeGen and TurboGrid, which are suitable for the definition of impeller geometry and efficient mesh generation.

Inlet pipe

The geometry of the inlet pipeline was created in SpaceClaim. The inlet pipe contains a hub that forms a boundary layer at the corner of the blade, as the installation of the upstream inducer is expected to have this hub shape. Next, a computational mesh was created for this domain using the Ansys meshing tool. The boundary conditions for meshing were set and the meshing method chosen was a tetrahedral meshing, which can easily accommodate complex geometries at the cost of lower accuracy and higher computational power requirements. An inflation function was applied to the domain walls to ensure a higher quality mesh near the walls, where high values of velocity gradients will be due to boundary layer evolution. At the same time, these conditions were applied to the surface acting as the interface with the impeller domain to minimize the effect of interpolation of the two domain meshes.

Spiral

The spiral geometry was created based on an in-house program from the Viktor Kaplan Department of Fluid Engineering, which generates spiral sections consisting of Bezier curve segments based on the outlet diameter and width of the impeller combined with the pump flow rate. These curves were then used to create design points whose coordinates were

imported into the PTC Creo 5 environment. From there, the points were again used to create curves, which were further modified by creating the necessary rounding and used to create a surface describing the hydraulic region of the spiral. Next, the tongue of the spiral was modeled based on the theory of shockless inflow. The inlet geometry of the spiral must exactly match the outlet shape of the impeller domain. Therefore, a cylindrical surface for the spiral inlet was created and was divided in width for the subsequent creation of boundary conditions. After suitable surface modification, the spiral was transformed from a planar to a volumetric body. As a final step, the geometry of the outlet pipe was added to further distance the outlet boundary condition from the region of interest. [37, 38]

Impeller

The impeller is very difficult to model in conventional CAD software. It is convenient to use curves to describe its geometry. For the purpose of this thesis, Bezier curves were chosen to be used extensively. Ansys provides a specialized tool, Ansys BladeGen, for creating rotating machine geometry. In BladeGen, the input and output diameters of the impeller and its output width are defined together with the number of blades and their angles. These include the angle of attack and the outflow angle. The blade geometry can be divided into several curves along its span. This way, it is possible to define a variation of the angle of attack along the span to correspond to the appropriate velocity triangles, while also defining a different wrap angle to ensure the manufacturability of the blade. It is also possible to define the thickness of the blade with respect to stress strength. All of these values can be defined as a function of the longitudinal position of the blade by the means of a Bezier curve.

BladeGen is then able to export a fluid domain model of the impeller, which is automatically trimmed to contain only one instance of the periodic geometry. A periodic boundary condition can be applied to it later to reduce the computational power requirement.

The computational mesh for the impeller domain was created in the Ansys TurboGrid environment, which is a specialized tool for creating computational meshes for rotating machines. It works on the principle of predefined domain decomposition , which allows it to be filled using hexahedral elements, which generally achieve higher computational accuracy while significantly reducing the computational effort. TurboGrid requires the input geometry to have a properly defined naming of the surface features. It allows for increased cell density in regions where significant velocity gradients can be expected. However, its disadvantage is that it is limited in the precise definition of the grid, for example, at the trailing edge of the impeller blades.

Boundary conditions

The definition of the boundary conditions is done in the Ansys CFX preprocess environment. Their defined locations have been set as shown in Figure 8.3 with their values corresponding to Table 8.1.

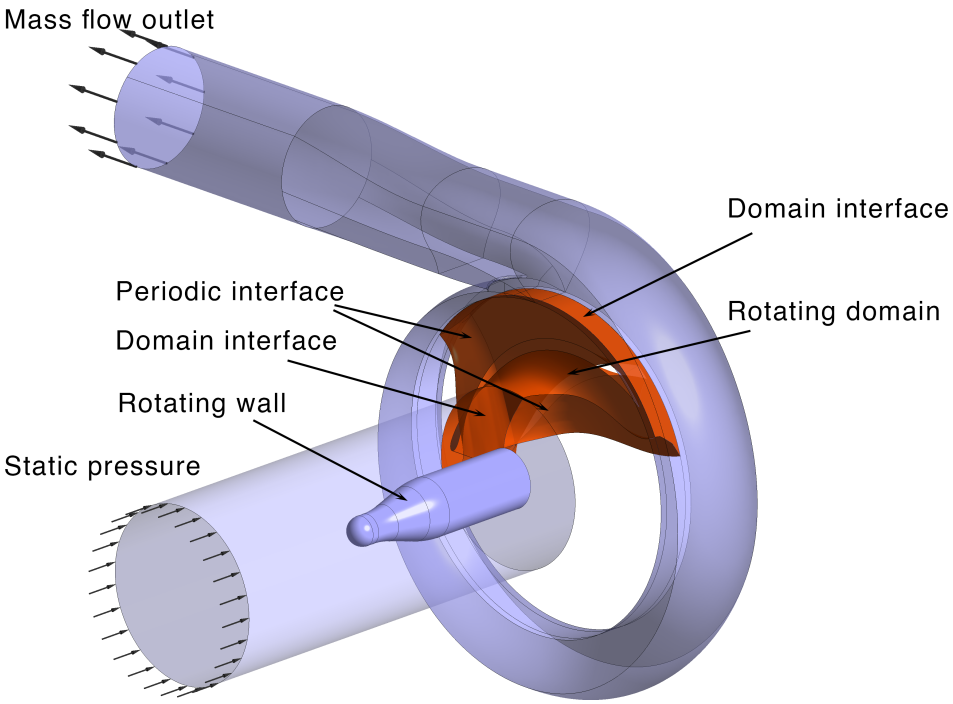

Figure 8.3: Complete geometry along with boundary conditions used for CFD assessment of radial-pump design

With this computational mesh configuration, the y^+ variable takes on values ranging from 20 to 120 on all the significant walls of the pump geometry. See Figure 8.4. Thus, the proper behavior of the Scalable wall function used in cooperation with the $k-\epsilon$ turbulence model can be expected.

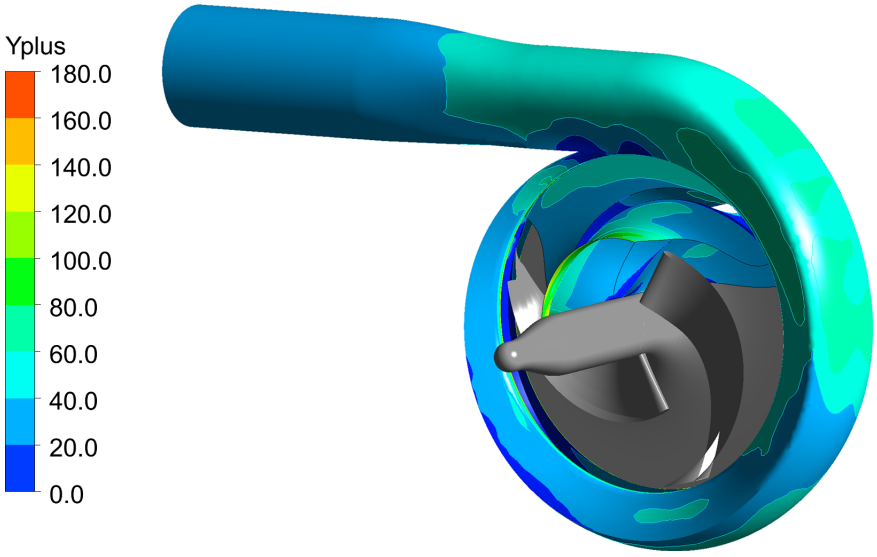

Figure 8.4: Distribution of Yplus variable across the radial-pump wall

For the purpose of this simulation, the wall surfaces figuring in the wall function were assumed to be perfectly hydraulically smooth.

8.5.2 Results

In order to achieve high hydraulic efficiency, the pump needs to minimize swirling inside its channels. Therefore, there is an effort to have a smooth monotonic flow across all wetted surfaces of the hydraulic fluid path. The cover disc and carrier back were thus modeled using Bezier curves to allow for a smooth transition from axial to radial flow, creating a meridian shown in Figure 8.5. The resulting shape allows for a smooth, monotonic pressure build-up inside the impeller.

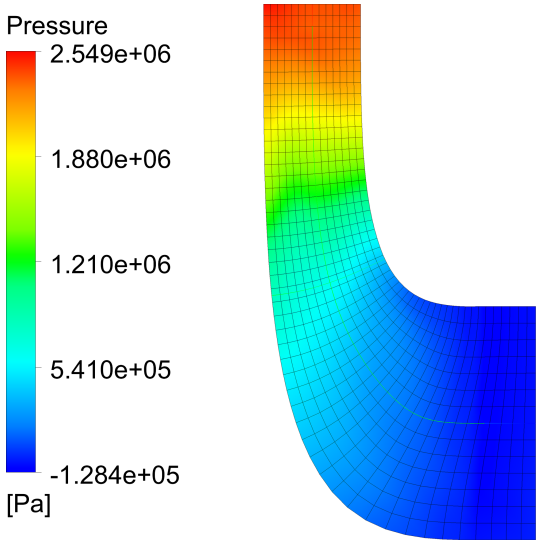

Figure 8.5: Distribution of static pressure across the meridian section of the radial-pump design

A single-phase fluid flow model was used to determine the $Q - H$ characteristics of the pump. Subsequently, the static pressure distributions inside the pump were evaluated. Based on this, preliminary areas with a risk of cavitation occurrence were determined and are shown in Figure 8.6.

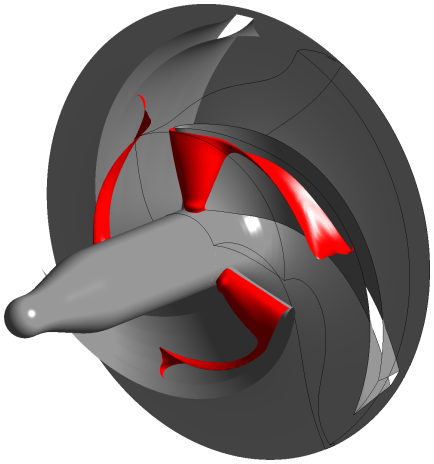

Figure 8.6: Display of a volume susceptible to cavitation development during nominal operation of the radial-pump design at a suction pressure of 2 bar

As expected, these areas were mainly located on the suction side of the leading edge of the blades. To some extent, it was possible to control the size of these areas by a suitable choice of blade incidence angle. Flow curvature at the blade leading edge can be seen in Figure 8.7. However, in this case, it was not possible to reduce these low-pressure areas enough to ensure safe operation at the required static suction pressure of the pump. At the radial stage inlet of the pump, a higher value of static fluid pressure must be ensured.

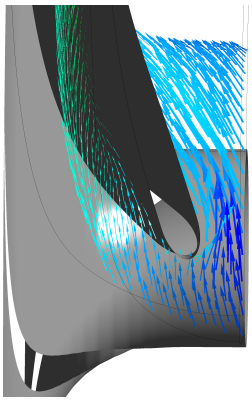

Figure 8.7: Flow direction on the leading edge of the radial-pump blade

However, the hydraulic efficiency of the pump is determined by the flow not only inside the impeller but rather by the flow along the whole hydraulic path. Design flow direction can be observed in Figure 8.8. It is therefore important to ensure that the volute is functioning correctly. A properly designed volute does not introduce unnecessary swirl and friction losses to the fluid. It is important that the volute has a shockless tongue slope at the design point. Its slope is based on the ratio of the circumferential and meridional velocity components at the impeller discharge and the assumption of preserving the flow slope across the bladeless diffuser downstream of the impeller.

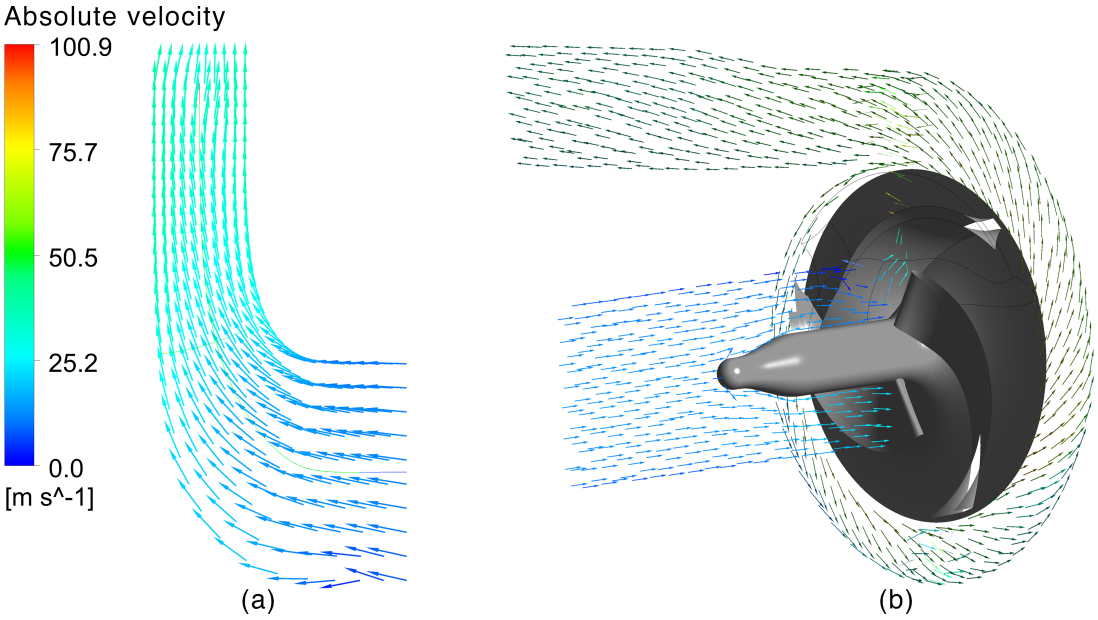

Figure 8.8: Velocity vector distribution field in radial-pump design

8.5.3 Splitter blades influence

Due to the expected small impeller dimensions and the large pressure increase, a high amount of specific energy is transferred onto each blade. The blades are outside their optimum operating range when loaded in this way, and increasing the number of blades can be expected to increase the pump efficiency and performance. Therefore, a comparison was made between a radial stage with only three blades and a radial stage with three additional splitter blades. The splitter blades reduce the flow area of the pump, which increases flow speed and decreases static pressure. It is therefore important to place the blades in an area where there is no risk of cavitation developement.

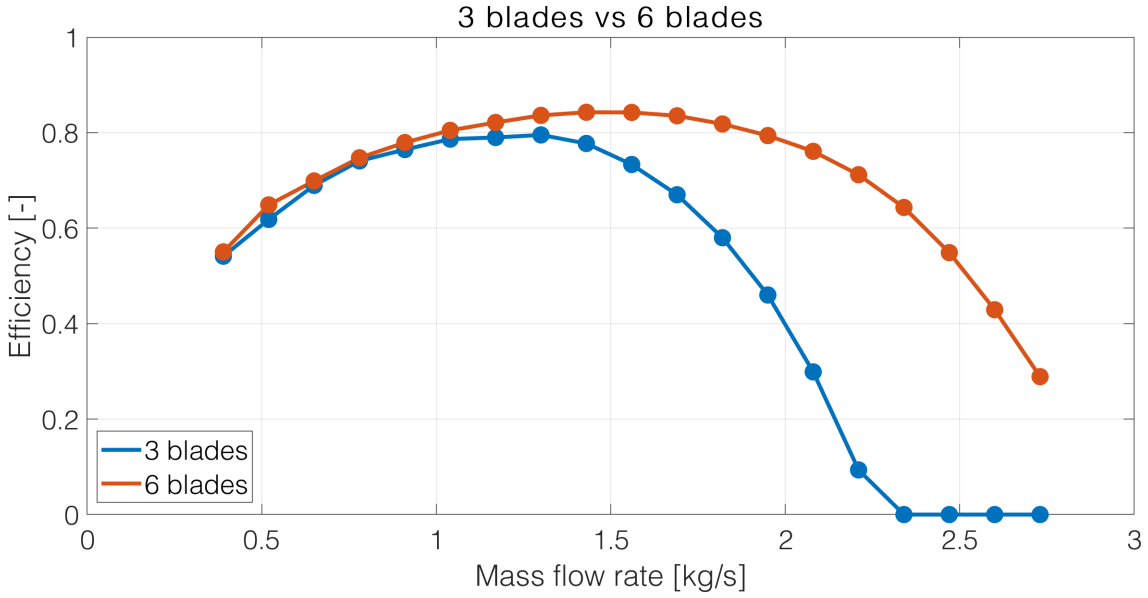

Figure 8.9: Efficiency comparison between impellers with three and six blades

The splitter blades leading edge lies at 30 percent of the main blade length and have identical geometry as a main blade. They are positioned 20 percent closer to the suction side of the main blades than the pressure side.

The comparisons in Figures 8.9 and 8.10 show an increase in maximum pump efficiency and performance. The smaller pressure gradient handled by each vane has also increased the delivery head of the pump. This effect would be even more pronounced with an open impeller, as the greater pressure difference at the side of each blade would induce a higher bypass at the blade tip gap.

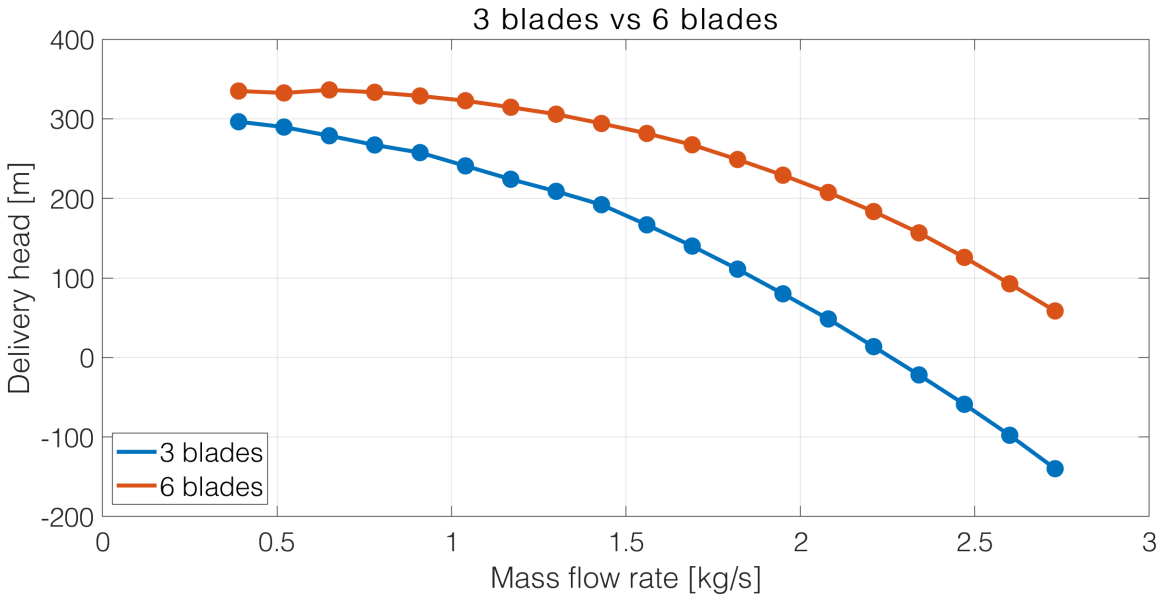

Figure 8.10: Delivery head comparison between impellers with three and six blades

At the same time, the splitter blades limit the development of secondary counter-rotating vortices in the impeller channels at off-design operating point, thus stabilizing the impeller operation outside the optimum flow rates. The resulting pump then has a wider operating range as seen in Figure 8.9.

Chapter 9

Axial stage design

An inducer is an axial pump introduced to a radial stage to increase suction pressure. Axial pumps are less efficient than radial pumps. Therefore, the inducer is only designed to increase the pressure enough to guarantee the reliable operation of the radial stage. Due to the low power of the inducer, its design is often simplified and the manufacturer does not address its efficiency. However, our application will be optimized for appropriate operating dynamics and maximum efficiency.

Its design is complex and an optimized design requires an extensive study of the methods used and the phenomena that can improve efficiency. The basic design of the axial pump, like the radial stage, is based on 2D vane stall theory, which uses a series of relationships based on potential flow. These relationships are then corrected by appropriate coefficients for the actual application. Based on these relationships, a script was created in MatLab, the output of which is a mathematical description of the pump vane.

9.1 Target parameters

Since the inducer is in series with the radial stage, it can be considered to handle the same flow. Since it is mounted on the same shaft, it has the same speed. These two parameters sufficiently define the geometry of the inducer inlet. Due to its efficency lower than the one of a radial impeller, it is recommended to process only 10-15 percent of the total pressure gradient of the pump group in this axial stage. Though in our case, it is possible to design the inducer considering the pressure rise required for cavitation elimination based on the previous radial stage simulation. With these parameters and assumptions, it is possible to define the blade geometry at the outlet of the axial stage.

$$H = \frac{\Delta p}{\rho \cdot g} = 21.8\, m \tag{9.1}$$

The target delivery head of the proposed inducer (see 9.1) is chosen to be 21.8 metres for the liquid used. This value is based on the pressure rise required for proper operation of the radial stage downstream of the inducer.

$$n_s = 3.65 \cdot \frac{n \cdot \sqrt{Q}}{\sqrt[4]{H^3}} = 770.6\, min^{-1} \tag{9.2}$$

Such a pump has a specific speed (see 9.2) of 770.6 per minute. For this value of specific speed, the use of an axial inducer design seems to be optimal. Table 9.1 lists the parameters that an axial inducer should achieve as well as the characteristics of the pumped fluid for the purpose of its design.

Table 9.1: Axial inducer target design parameters

Rotating speed	70000	rpm
Hydrogen peroxide	87-98%	H_2O_2
Density	1400	$kg \cdot m^{-3}$
Dynamic viscosity	0.00125	$Pa \cdot s$
Vapour pressure at 20°C	216	Pa
Mass flow rate	1.3	$kg \cdot s^{-1}$
Pressure gain	3	bar
Suction pressure	2	bar

9.2 Analytic design

When designing inducers, it is advantageous to use the so-called pressure head rise ψ, which is based on the required head and the circumferential speed of the inducer, as described in equation (9.3).

$$\psi = \frac{H \cdot g}{u_1^2} \tag{9.3}$$

The pressure head rise proves to be a decisive factor in the selection of a suitable pump design. Based on its value, axial pumps can be divided into low pressure rise and high pressure rise pumps, where the threshold between these definitions is $\psi = 0.15$. These pumps can then, as shown in Figure 9.1, vary further in design depending on the required pump characteristics, the material used, and the arrangement of the feeding line.

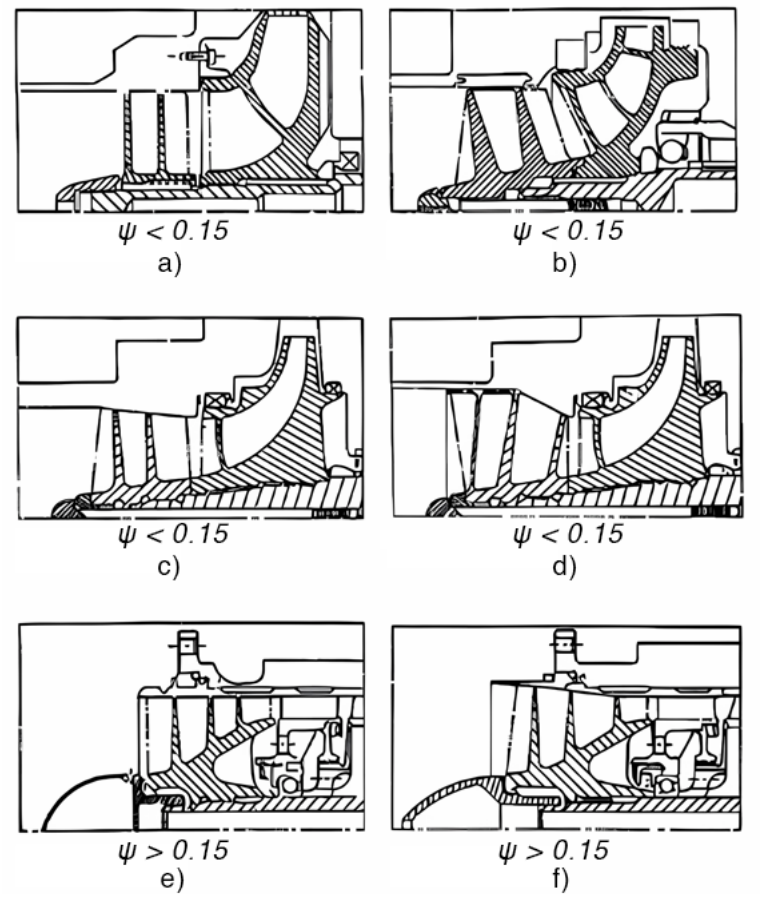

Figure 9.1: Comparison of basic inducer design types: a) Low-head inducer with cylindrical tip and hub, b) Low-head inducer with cylindrical tip, tapered hub, c) Low-head inducer with a tapered tip and hub, d) Low-head inducer, shrouded, e) High-head inducer with cylindrical tip, tapered hub, f) High-head inducer with a tapered tip and hub [24]

Inlet area

When designing the inducer inlet area, the flow coefficient ϕ, a dimensionless parameter used to compare different pump designs, can be applied. This coefficient is defined as the ratio of the inlet meridial flow velocity to the circumferential inducer velocity at the maximum diameter, see equation (9.4).

$$\phi = \frac{c_{m1}}{u_1} \tag{9.4}$$

A typical range of the flow coefficient for fuel pump inducers with high demands for low NPSH is $0.05 < \phi_1 < 0.14$. The inlet area and pump diameter are then selected based on this value.

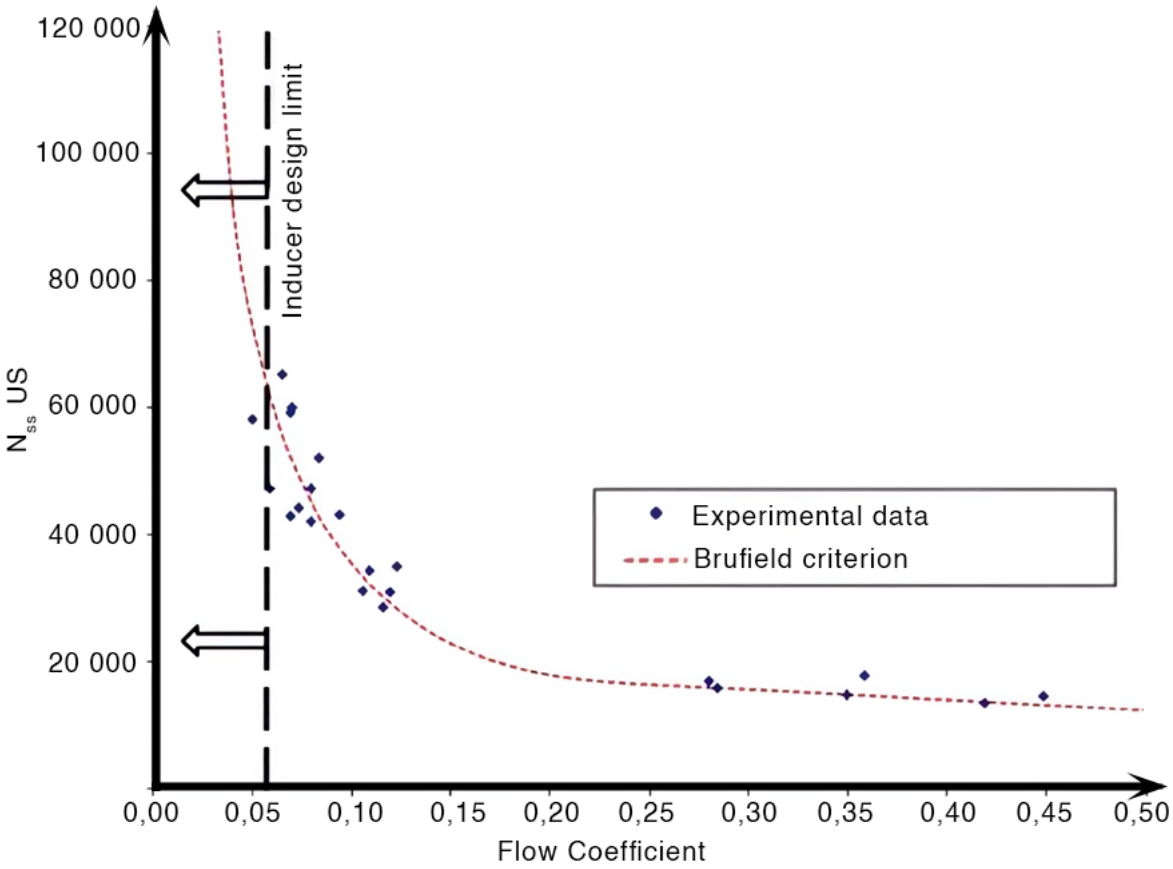

Figure 9.2: Brufield criterion for the suction head as a function of flow coefficient [31]

The Brumfield criterion (see Figure 9.2) allows visualization and estimation of the inducer's suction capabilities. In general, the lower the flow coefficient, the higher the specific speed, and therefore the lower the NPSH value. However, the pump design is limited by $\phi < 0.05$ because strong flow instabilities form at lower flow coefficient values. In particular, the formation of a recirculation region is an issue. The low meridional velocity at low flow coefficient values necessitates a high blade leading edge angle. Such a blade then significantly limits the flow area and the flow is more sensitive to the formation of a cavitation region behind the leading edge.

On the other hand, the design of inducers with low flow coefficients is not impossible. However, proper modification of the incoming flow is required. For example, guide vanes restrict the formation of a recirculation vortex at the pump inlet.

Blade angles

The design of the inducer is in many respects similar to that of a radial stage pump. It is based on the conventional form of the Euler pump equation (9.5). This gives the increase in the specific energy of the fluid based on the velocity triangles. Based on the required pump parameters, the rate of increase in specific energy and hence fluid velocity can be determined. From these, the blade angles can then be derived.

$$\Delta Y = \frac{\Delta p}{\rho} = u_2 \cdot c_{u2} - u_1 \cdot c_{u1} \tag{9.5}$$

For axial stage pumps, however, it is problematic to determine the reference diameter against which the equations apply. Euler's pump equation is a form of the conservation of energy law and the specific energy is supplied to the fluid in the form of kinetic energy, which may then be transformed into pressure energy. It is therefore convenient for the calculation to find the reference diameter of the pump as one which, at constant velocity distribution at the pump inlet and outlet cross-sections, achieves the same specific energy as the energy of flow with real velocity distribution across the cross-section. Resulting diameter is shown in formula (9.6).

$$D_s = \sqrt[4]{\frac{D_0^4 + d_0^4}{2}} \tag{9.6}$$

This diameter can then be used to calculate the inducer's circumferential velocity (9.7). In case the flow area changes along the meridian, this equal diameter must be determined for all relevant sections of the pump.

$$u = \pi \cdot D_s \cdot n \tag{9.7}$$

Using the velocity triangles, the angle of attack (9.8) and the trailing edge angle (9.9) of the blade are determined by this procedure. These must however be corrected using an incidence angle at the leading edge and a deviation angle at the trailing edge of the blade. Formulas can be seen below:

$$\beta_1 = \arctan \frac{c_{m1}}{u_1 - c_{u1}} + i \tag{9.8}$$

$$\beta_2 = \arctan \frac{c_{m2}}{u_2 - c_{u2}} - d \tag{9.9}$$

As mentioned in the previous chapter, the pumps achieve minimum viscous losses and maximum efficiency when the blade angle changes smoothly. For axial stages, it is practical to employ the use of linear blade angle change, which is a common practice in pumps that maintain flow area.

To increase pump efficiency, there is also an effort to utilize the effect of centrifugal forces to raise the pressure in axial machines. However, this is only possible when changing the flow area of the pump. In addition, this confusor shape of the flow path leads to a more uniform velocity and pressure field, especially near the hub. It is advisable to define a series of points along the pump meridian and to determine the flow area at each of these locations. It is then possible to determine the development of the blade angle so that the blade is as smooth as possible for the flowing fluid.

9.3 Design features

Axial pumps are specific in their design and several features can be used in their design to increase their efficiency and operating stability. As these pumps are highly susceptible to relative velocity angles, it is advisable to focus on maintaining the correct relative blade angles. These are particularly critical in the area of the end of the blades on the shroud, where there is a significantly developed boundary layer in the supply pipe.

9.3.1 Slanted inlet

The inlet of an axial flow pump is often angled or slanted (as shown in Figure 9.3) to improve the inlet fluid flow and minimize the negative effects of eddies, boundary layer turbulence, and gasses encased in the fluid.

If the inlet is angled, it directs the incoming fluid at an angle to the pump axis. This helps to create an eddy motion of the fluid, which helps to increase flow and improve pump efficiency. This also proves to be beneficial when trying to minimize cavitation development inside the pump, as the center of the flow enters the pump first. It then accelerates and also increases the speed of the pipe boundary layer, which is then more predictable and its velocity corresponds closer to that of the freestream. This means the incidence angle at the leading edge of the blade is lowered without significant curvature of the blade end. The swirling motion also helps reduce the formation of eddies that can lead to cavitation and other problems that reduce pump performance. The angled inlet also helps reduce the amount of air entering the pump. Air can reduce pump efficiency and cause cavitation. A sloped inlet helps to separate the gasses from the liquid and reduce the amount of gasses entering the pump.[21, 26]

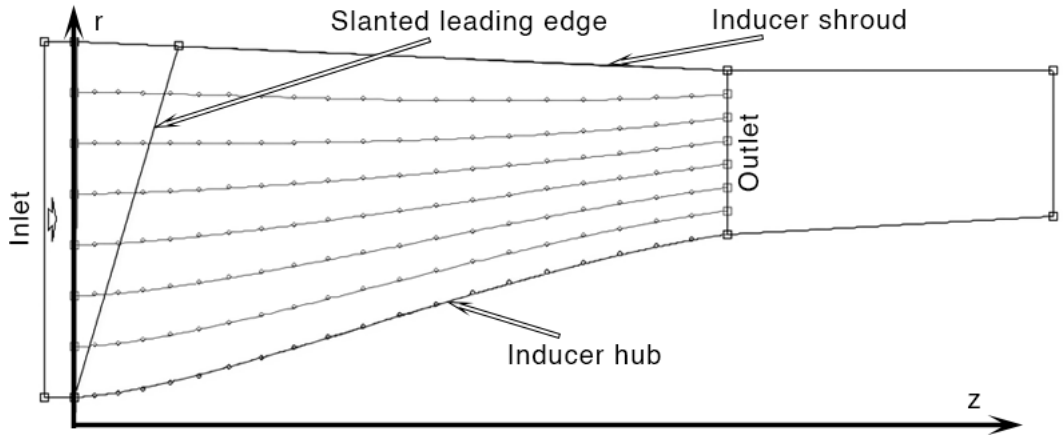

Figure 9.3: Meridial section of the axial pump with slanted inlet design [10]

9.3.2 Blade backsweep

The main reasons for the backward bending of the blades in inducers are to reduce the occurrence of cavitation and to increase efficiency. The efficiency is increased by minimizing

the inlet pipe boundary layer influence through bringing the free-flowing fluid into contact with the blade before the fluid of the pipe boundary layer. Thus, it can transfer energy to the boundary layer and accelerate this fluid. Its velocity then corresponds more closely to the free stream velocity and is closer to the parameters used to determine the blade angle of attack. The backward curvature of the blades also ensures a more even distribution of static pressure in the machine, which reduces cavitation formation. This also indirectly reduces the machine's noise and vibration. The resulting inducer can then achieve higher efficiency and reliability.[21, 26]

Blade backsweep shown in Figure 9.4, can be created when defining blade wrap angle in CAD. However, it can be difficult to design reasonable blade profiles throughout the whole meridian length and it adds difficulty to its manufacturing.

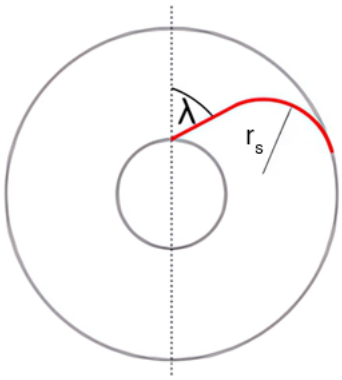

Figure 9.4: Front view of the inducer blade leading edge geometry [26]

9.3.3 Airfoil blade profile

Airfoil shapes are commonly used in axial pumps as they effectively create lift and reduce drag, both of which are key factors in efficient axial pump performance. One of the airfoil benefits is its stall resistance. In the case of the pump, this means that the low-pressure area behind the leading edge is smaller than a similar straight pump blade at the same incidence angle.[21]

Since an axial pump works by accelerating the axial flow stream's tangential velocity while increasing its specific energy. The aerodynamic wing shape of the pump rotor blades allows for efficient acceleration of the fluid, resulting in higher flow rates and pressures. The shape of the airfoil also helps to reduce resistance, minimizing losses and increasing overall efficiency. In addition, the shape of the airfoil allows for better control of fluid flow through the pump, which is important for maintaining stable operation and preventing cavitation.[21]

The design of the airfoil shape is defined by the set of parameters as seen in Figure 9.5, and can be optimized for specific operating conditions such as high flow rates or high pressures with changes in maximum thickness and camber.

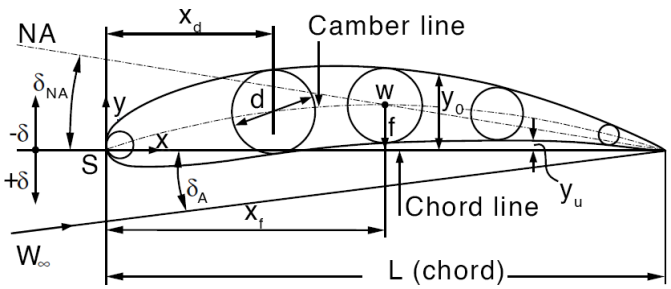

Figure 9.5: Airfoil profile defining parameters [21]

9.4 Design specifications

The design of the axial stage was based on the geometry of the subsequent radial stage. This matches the diameter of the inducer shroud, see Table 9.2. At the same time, however, an attempt was made to exploit the effect of centrifugal forces to increase the pressure. Therefore, the diameter of the hub increases streamwise.

Table 9.2: Axial inducer design dimensions

Number of blades	3	
Inlet shroud diameter	12	mm
Inlet hub diameter	3	mm
Outlet shroud diameter	12	mm
Outlet hub diameter	8	mm

This change in the hub diameter causes a change in the flow path cross-section of the pump, and the blade angle must be adjusted so that the increase in the circumferential velocity of the pumped fluid is as even as possible. At the axial stage outlet, the aim is to achieve a uniformly rotating fluid flow. For this purpose, it is necessary to shape the blade as a function of its radius. Similarly, the blade's leading edges need to be shaped to ensure the correct back sweep, resulting in improved cavitation properties. It is therefore necessary to divide the blade into a minimum of 5 layers as a function of the radius, with each layer having a precisely defined blade pitch angle and a blade wrap angle at each point of the blade. The resulting angles of blade's leading and trailing edges can be seen in Figure 9.6.

It is important to note, that because of streamwise hub diameter change, same blade span fraction does not correspond to the same diameter on both edges.

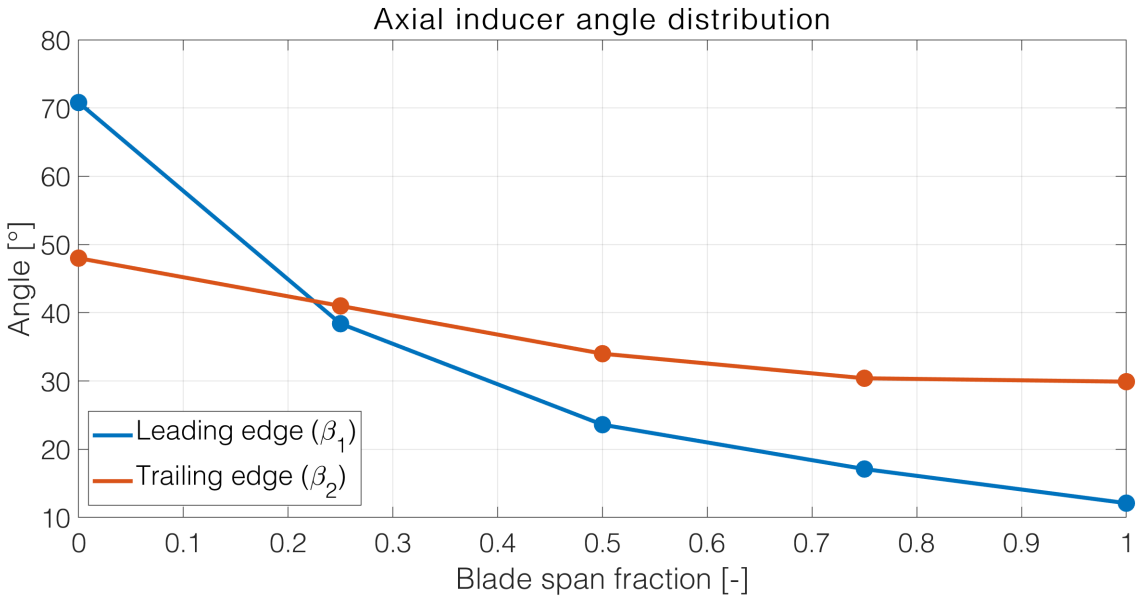

Figure 9.6: Axial inducer's blade leading and trailing edge angles

9.5 CFD solution

The design of the inducer was validated by CFD calculations similarly to the radial stage design. In particular, the curvature control of the flow through the inducer is important, but also the pressure field development at the intake. The inducer always operates in the lowest pressure region and the cavitation properties of the pump are therefore based on inducer's design.

9.5.1 Preprocess

The axial stage calculations, similarly as for the radial stage, were performed in Ansys Workbench, which provides all the resources needed for this task.

Inlet pipe

The inlet pipe geometry is very similar to that used for the radial stage design. It is a cylinder with a diameter of 12 millimeters and a length of 50 millimeters. This length is essential to allow the flow field to develop in a realistic manner. A shorter inlet channel could limit the development of vortices upstream of the inducer by the presence of inlet boundary condition, compelling constant pressure distribution.

The inlet duct also contains the inducer hub tip in the shape of a hemisphere.

The computational mesh is created using Ansys Workbench Meshing using the multizone algorithm. The resulting mesh has a very regular structure and is made up of purely hexahedral elements oriented in the flow direction.

Outflow pipe

The outflow domain is a pipe, shaped by an interring, where its outer diameter corresponds to the diameter of the inducer shroud and its inner diameter corresponds to the outlet diameter of the inducer hub. Its length is 80 millimeters because it is important to capture the swirl of the flow at the outlet of the inducer, which often entails the development of vortices. In order for these vortices to develop, a large distance from the outlet boundary condition is required.

The computational mesh is created in the Ansys Workbench Meshing environment, where the domain is divided into 4 quadrants and then the number of elements that make up each edge of the domain is assigned. The resulting mesh is then fully structured and is made up purely of hexahedral elements oriented in the direction of flow.

Inducer

The geometry of the inducer was created in Ansys BladeGen, which allows the parametric design of turbomachine components.

The shape of the pump meridian was created using Bezier curves describing the shape of the hub and the inducer shroud. Since the inducer is supposed to be used in cooperation with the radial stage of the pump, its inlet and outlet surfaces are purely axial to allow for compact packaging. This may reduce the efficiency of the inducer since the fluid has to change its radial velocity twice. Another option would be to have a diagonal inducer outlet and a diagonal radial stage inlet. That would necessitate a larger pump, but could be interesting for future research.

The shape of the blades is mainly limited by the leading and trailing edge angles, the values of which are based on the analytical design. However, due to the increasing diameter of the inducer hub, it is not possible to use a conventional linear angle transition. The slope angle along the blade was therefore described by a Bezier curve, which allows smooth fluid flow without excessive frictional losses. Like the slope angle, the blade wrap angle is also defined. Because of the need to vary the leading edge angle and trailing edge angle as a function of radius, it is necessary to define at least five control layers in which the blade is defined. These layers are also subsequently used to define the back sweep of the blades leading edge.

The model created in BladeGen is then loaded into the TurboGrid environment, which is a parametric software designed to create high-quality rotating machine meshes. The resulting mesh is then made up of purely hexahedral elements of high quality. Such a mesh promotes solution stability and speeds up computation.

Boundary conditions

The boundary conditions of the calculation were defined in Ansys CFX Pre and their locations can be seen in Figure 9.7. The values of each boundary condition are defined in Table 9.1.

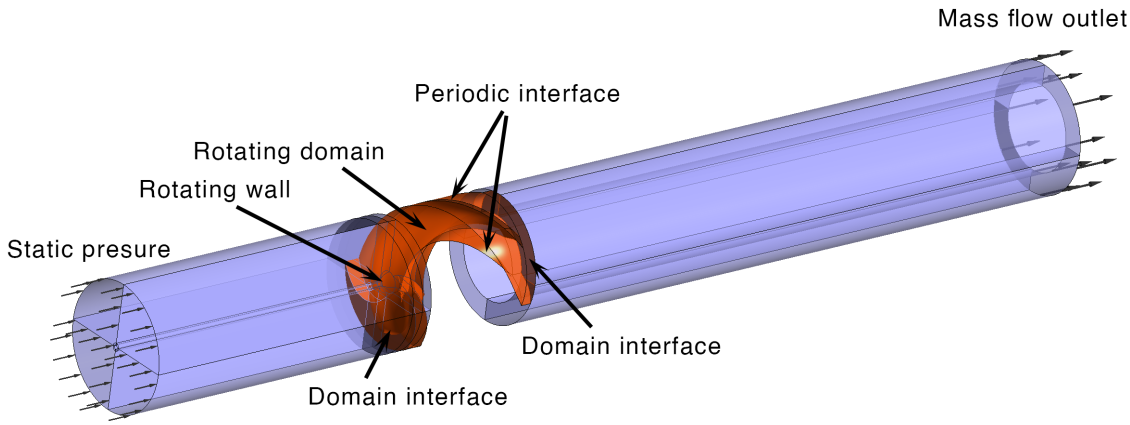

Figure 9.7: Boundary condition definition in axial stage simulation

For the purpose of this simulation, the $k - \epsilon$ turbulence model in combination with the scalable wall function was employed again. The wall function is set up to consider walls as perfectly smooth. For this configuration, it is advisable to keep the value of y^+ on the domain walls between 20 and 240.

As done in the case of the radial stage, the single-phase simulation was done, since there is no need to accurately capture the cavitation occurrence.

Zero shear stress wall boundary conditions were used to define the outflow domain so that boundary layer friction does not introduce additional losses into the system.

9.5.2 Results

The fundamental parameters of the pump axial stage were calculated on the basis of a single-phase fluid model. These are delivery head and hydraulic efficiency. Based on a series of calculations, the dependencies of these performance parameters on the pump flow rate were determined. These can, together with radial stage values, be seen in Figures 9.8 and 9.9.

As expected, the axial stage of the pump has a much narrower working window than the radial stage. At flow rates below 60 percent of the design flow, it enters into unstable operation and the maximum possible flow is 130 percent of the design flow.

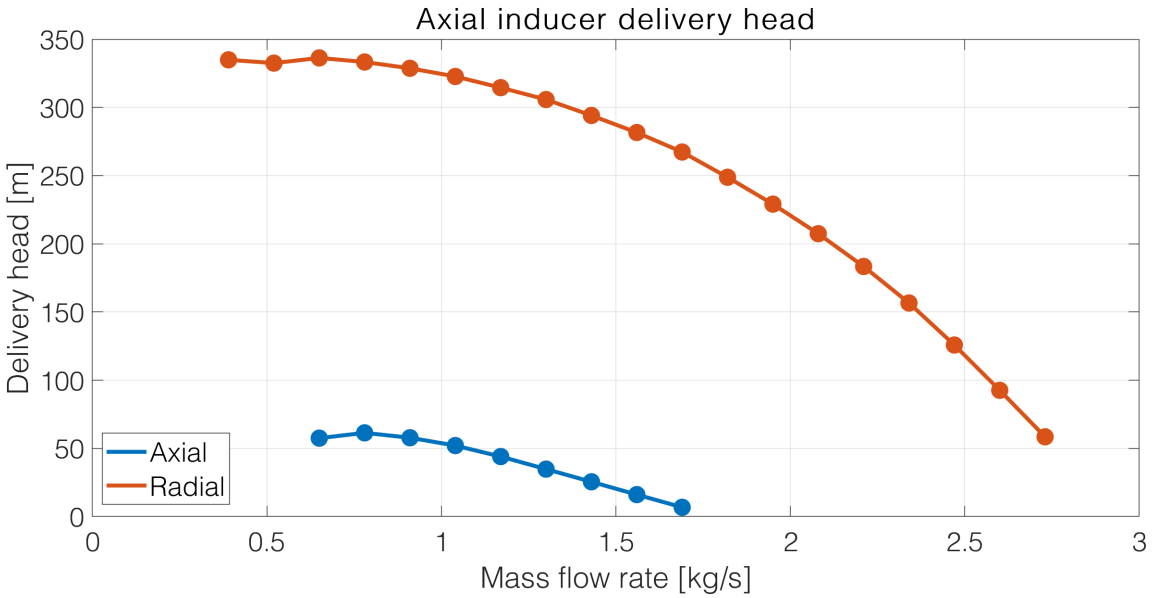

Figure 9.8: Axial stage delivery head characteristic

The axial stage pump achieves efficiencies up to 84 percent at 90 percent of the design flow. It is interesting to note that the optimum is not at the design point but rather a little lower, since the main purpose of the axial stage is to guarantee operation at low suction pressure without the presence of cavitation. The incidence angles at the blade leading edge have been tailored to this. It is therefore still advantageous for the pump to achieve 3 percent lower efficiency at the operating point because of this, as the design guarantees more reliable operation at low suction pressure.

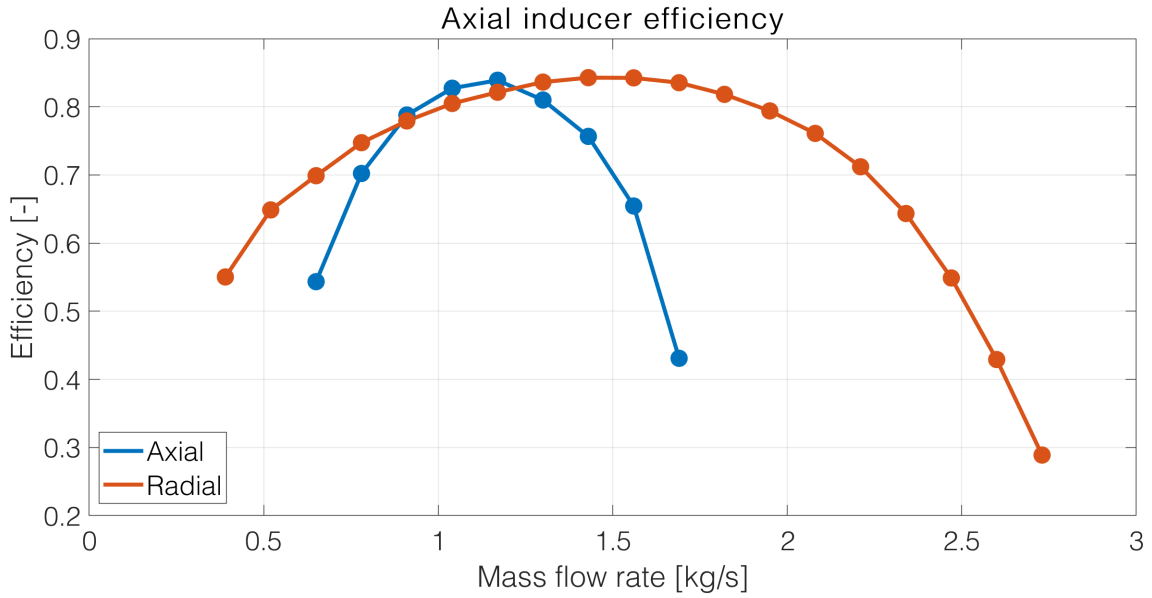

Figure 9.9: Axial stage efficiency characteristic comparison

Moreover, for this pump, efficiency is a secondary parameter, as it will be used in a system that is not running for a long period of time and its energy consumption may be somewhat neglected. An efficiency of 81 percent is satisfactory for this axial flow inducer.

The incidence angle determination is an iterative procedure based on monitoring the direction of the velocity vector near the leading edge of the impeller blades as seen in Figure 9.10. The blade pitch is adjusted so that the fluid does not have to change direction too quickly, which would result in a significant pressure decrease.

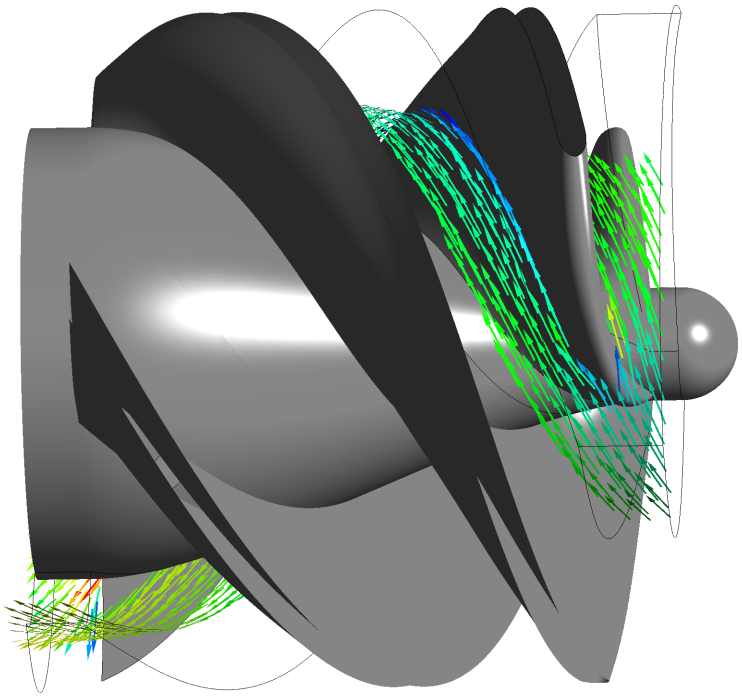

Figure 9.10: Flow direction near inducer blade at 50 percent blade span fraction

From the standpoint of blade angle of attack design, the effect of the boundary layer on the fluid flow velocity is strongly evident in hydraulic machines of such small dimensions. It is therefore necessary to compensate the blade angle of attack appropriately near the inlet wall. The fluid is significantly slower in this area and, despite the slanted blade leading edge, a vortex ring forms in the area just upstream of the blades in case an inappropriate angle of attack is used. This then limits the flow area for the fluid and changes the meridional velocity distribution at the inducer inlet.

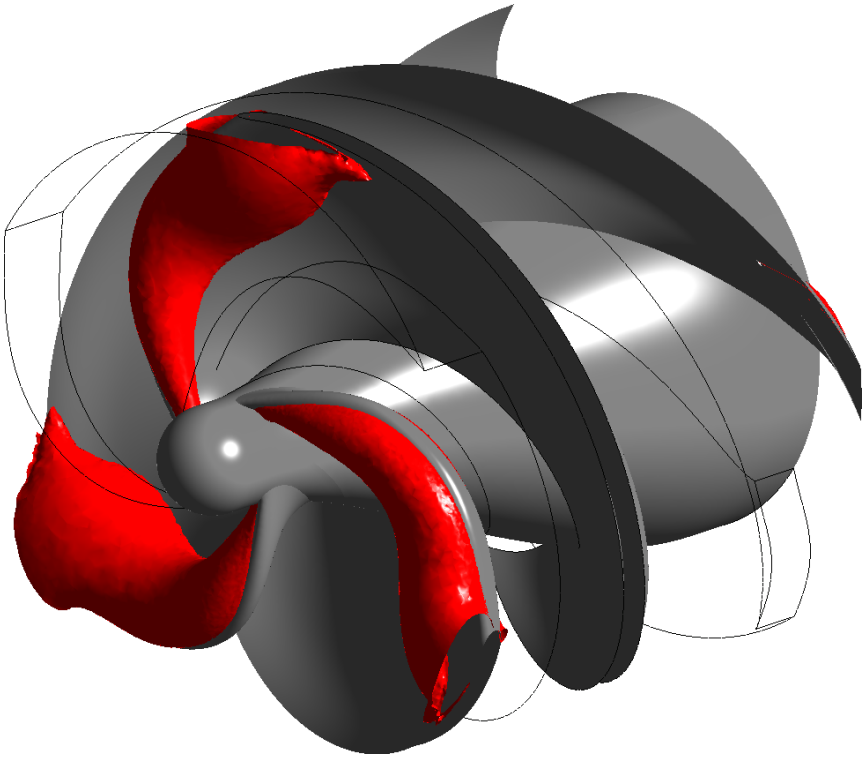

Figure 9.11: Low pressure region near axial inducer blade leading edge at optimum

Figure 9.11 shows the region where, according to the single-phase simulation, the pressure is lower than the saturation vapor pressure of hydrogen peroxide at the target inlet pressure. However, previous calculations and historical measurements indicate that the actual region of cavitation will be much smaller than the single-phase calculation suggests. They also indicate that the inducer is expected to operate reliably at the design point.

Chapter 10

Mixed stage design

For reliable operation at the required pump suction pressure, it is necessary to have a pump fitted with an axial stage. To achieve the required delivery head, a pump utilizing centrifugal forces in the radial impeller must be used. The main aim of this thesis is to combine these two impellers into one with the expectation that such a combined impeller will be smaller, lighter, and could achieve higher hydraulic efficiency due to the absence of a radial impeller blade leading edge.

10.1 Target parameters

The target parameters of this combined impeller are very similar to the radial stage design. The only change being the necessity to ensure operation at low suction pressure. These parameters can be seen in the following Table.

Table 10.1: Target parameters for the design of axial-radial impeller-pump

Rotating speed	70000	rpm
Hydrogen peroxide	87-98%	H_2O_2
Density	1400	$kg \cdot m^{-3}$
Dynamic viscosity	0.00125	$Pa \cdot s$
Vapour pressure at 20$^{\circ}C$	216	Pa
Mass flow rate	1.3	$kg \cdot s^{-1}$
Pressure gain	28	bar
Suction pressure	2	bar

10.2 Design specifications

As a final design, the combined impeller pump stage will use all the features that improve the performance of the axial and radial stages. From the analytical design, the parameters in Table 10.2 were derived. The impeller leading edge and trailing edge angles used are shown in Figure 10.1.

Table 10.2: Combined impeller design dimensions

Number of blades	3	(6)
Inlet shroud diameter	16	mm
Inlet hub diameter	3	mm
Outlet shroud diameter	24	mm
Outlet channel width	1.56	mm

The impeller has 3 blades that run throughout its entire length, as well as 3 more splitter blades of identical geometry added into the last 30 percent of the meridional area. A quarter-circle-shaped backward sweep with a radius of 3 millimeters is formed at the impeller leading edge. At the same time, the leading edge is inclined at the shroud by 2 millimeters relative to the hub. The blades of the suction area have an increased thickness to curve the fluid flow direction more effectively.

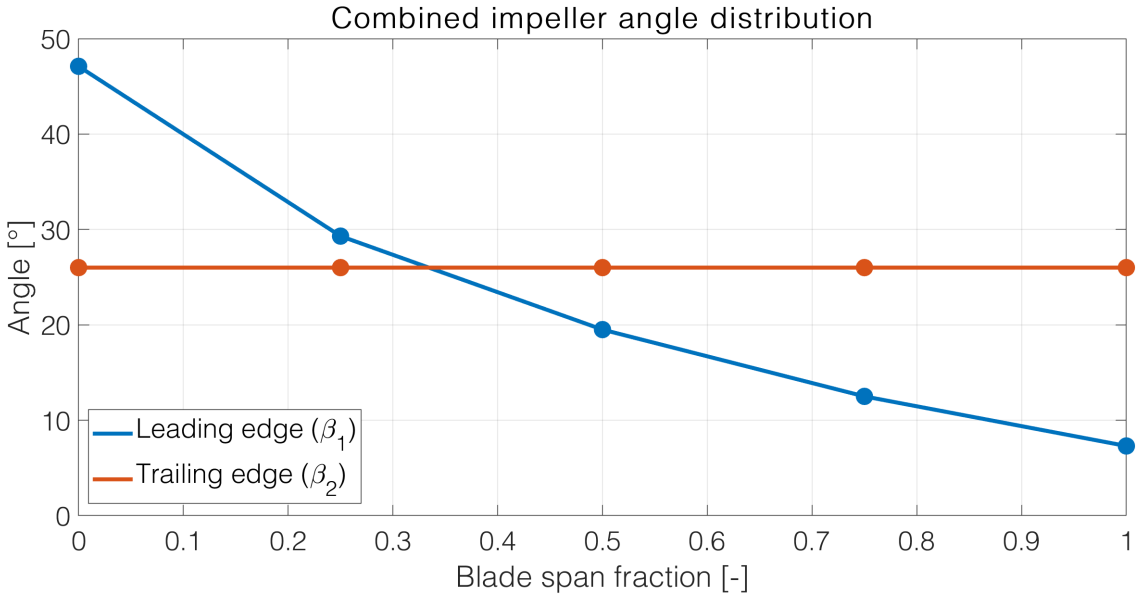

Figure 10.1: Combined impeller's blade leading and trailing edge angles

The meridian of the impeller is defined using Bezier curves, with the impeller inlet being purely axial and the outlet being purely radial.

In particular, the blade contours are problematic, as the transition from a complicated axial geometry at the inlet to the radial geometry at the outlet requires a significant change in blade angle across its span. This problem is solved by creating five layers on which the blade pitch angle, blade wrap angle, and blade thickness are defined. The evolution of the blade pitch is adapted to change the direction of the fluid flow as evenly as possible with changing meridional velocity. However, this shape is strongly constrained by manufacturing capabilities, so the blades have been modified to be less twisted than this design requires.

10.3 Performance characteristics

CFD simulations were used to evaluate the characteristics of the combined impeller pump. As shown in Figure 10.2, the design overestimates the requirements as it reaches a delivery head of 347 m at the design point. This value is so high to decide whether it is even possible to reach the delivery head required using an open impeller design as shown in chapter 10.4.

As shown in Figure 10.3, the combined impeller design, similarly to the axial stage, is characterized by a narrow operating window caused by the impeller inlet sensitivity to changes in incidence angle. Its efficiency then decreases rapidly, and the operation becomes unstable when the flow rate drops below 65 percent of the design point flow rate.

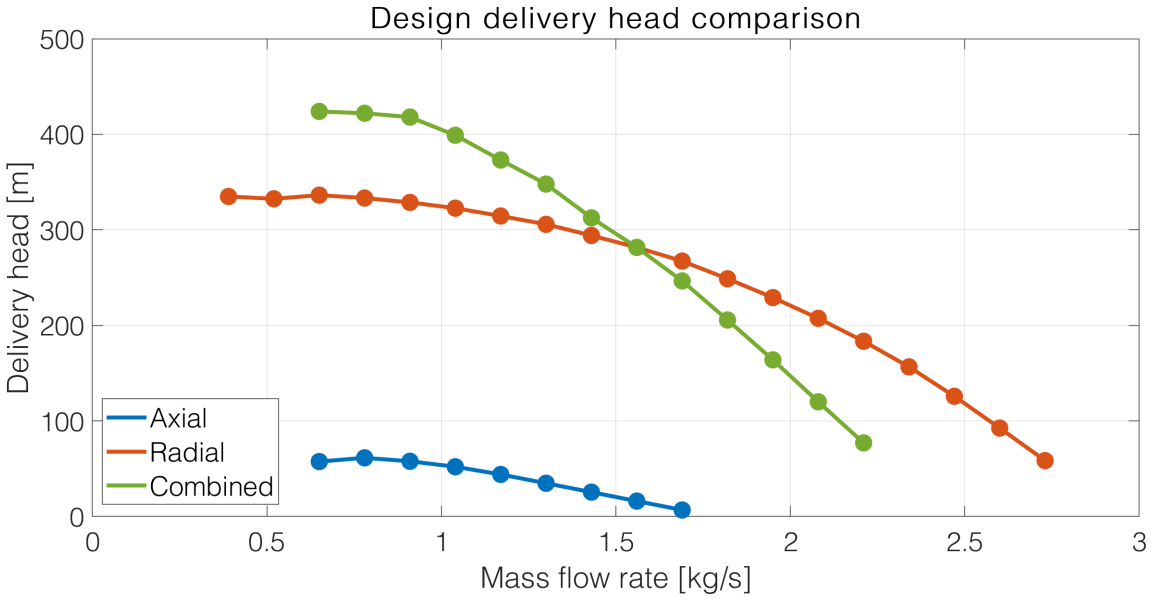

Figure 10.2: Delivery head comparison of different impeller designs

In addition, the impeller achieves higher maximum efficiency than the other designs, up to 94 percent. Interestingly, due to the reduction of the low-pressure region on the suction side of the blade leading edge, the pump's optimum point is shifted to slightly higher flow rates. The drop in efficiency at the design point is 0.3 percent compared to the optimum. This decrease is minimal and has little significance on the usability of the pump compared

to the fact that by adjusting the incidence angle, the pump can be run at significantly lower inlet pressures.

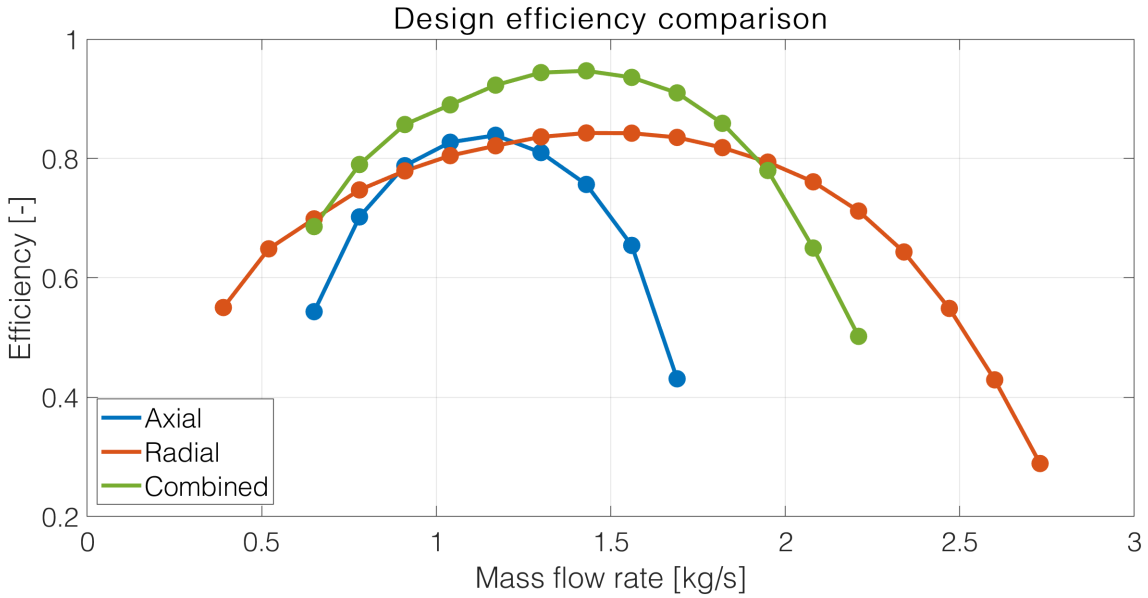

Figure 10.3: Hydraulic efficiency comparison of different impeller designs

It is important to note that the absolute values of delivery head and efficiency may be biased due to domain discretization and the effect of assumed simplifications of the fluid flow, such as turbulence model and domain interface definition. At the same time, hydraulically perfect smooth walls are assumed for the purpose of the simulations, which, especially for components of such miniature dimensions, cannot be guaranteed in reality. However, the results are useful in the sense that all calculations were performed under very similar conditions and therefore it should be possible to compare them with a high degree of confidence. On the basis of these results, it is, therefore, possible to see the change in the properties of the individual designs and to observe what direction to take in the design going further.

Should it be needed to know the exact values of the real delivery head and efficiency, it is recommended to validate the calculation setup on a similar pump on which these characteristics would have been measured.

10.3.1 Cavitation performance

A two-phase CFD calculation was used to determine the cavitation characteristics of the pump, which, in contrast to the single-phase calculation, includes the energy conservation law equations.

The Mixture Model scheme is used for energy transfer between phases and the Mass Transfer scheme is used for mass transfer modeling. Two phases have been set as the working medium. These are liquid hydrogen peroxide and gaseous hydrogen peroxide. The boundary conditions were modified by prescribing a value for the ratio of representation

of each phase at the input and output, which for the case of this problem was only liquid hydrogen peroxide at both boundary conditions.

The actual CFD calculation to determine the $NPSH_3$ was performed in a similar manner to the actual experiment. That is, the pump was run at a pressure at which cavitation did not occur and this pressure was gradually reduced until the delivery head of the pump dropped by three percent.

The calculation was carried out by first performing a static calculation of the flow in the impeller at the single-phase flow setting. Subsequently, the two-phase flow module was run in combination with the first-order turbulence numerics scheme. Once this calculation was relatively stable, the turbulence numerics scheme was switched to high resolution (second order).

However, since cavitation is a strongly time-dependent process, reliance cannot be placed on the results of the stationary calculation. Therefore, a transient calculation was performed. The time step duration was set such that the pump impeller was rotated by two degrees at each step. It turns out that this value provides a good convergence. Next, it was necessary to wait for the flow within the domain to stabilize. The calculation corresponded to two full revolutions of the impeller. With three blades, six periods are considered. The calculation was only terminated when two consecutive periods showed the same delivery head and efficiency pattern.

After the delivery head for a given suction pressure was stabilized and evaluated, the static pressure value at the inlet boundary condition was reduced. By this procedure, the values in Figure 10.4 were measured.

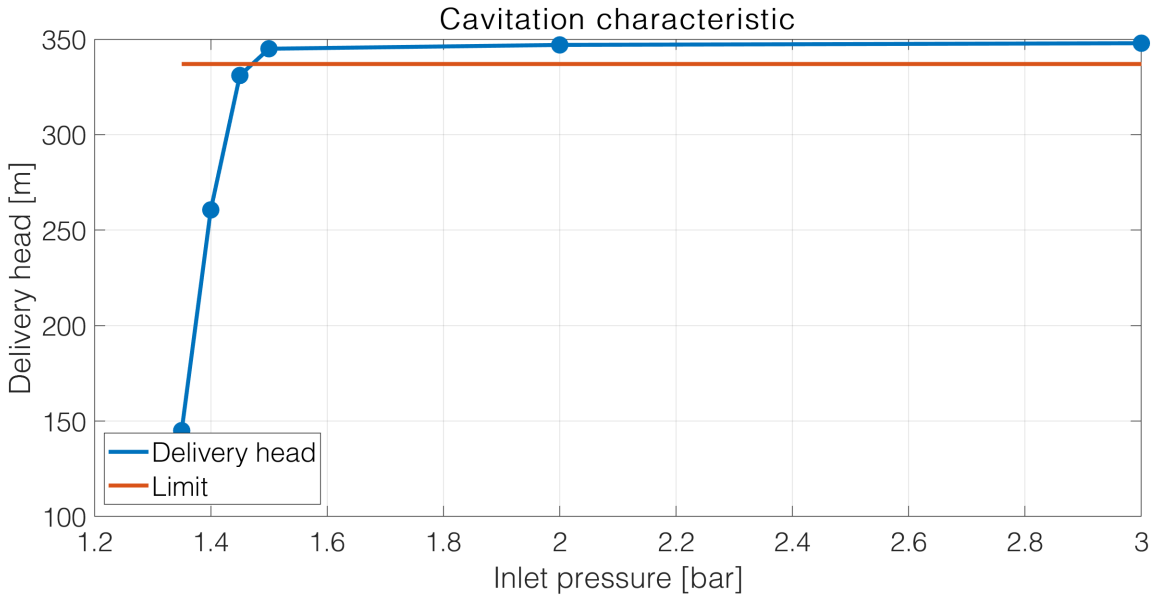

Figure 10.4: Delivery head dependency on inlet pressure for combined impeller design

The value of $NPSH_3$ was then determined as to match the conditions of a static inlet pressure at which the value of the delivery head drops by 3 percent. For this pump design, the

critical value of suction pressure at the design point appears to be 1.46 bar. How the value of the critical pressure depends on the pump flow rate is indicated in Figure 10.5, where it is directly expressed in $NPSH_3$ format.

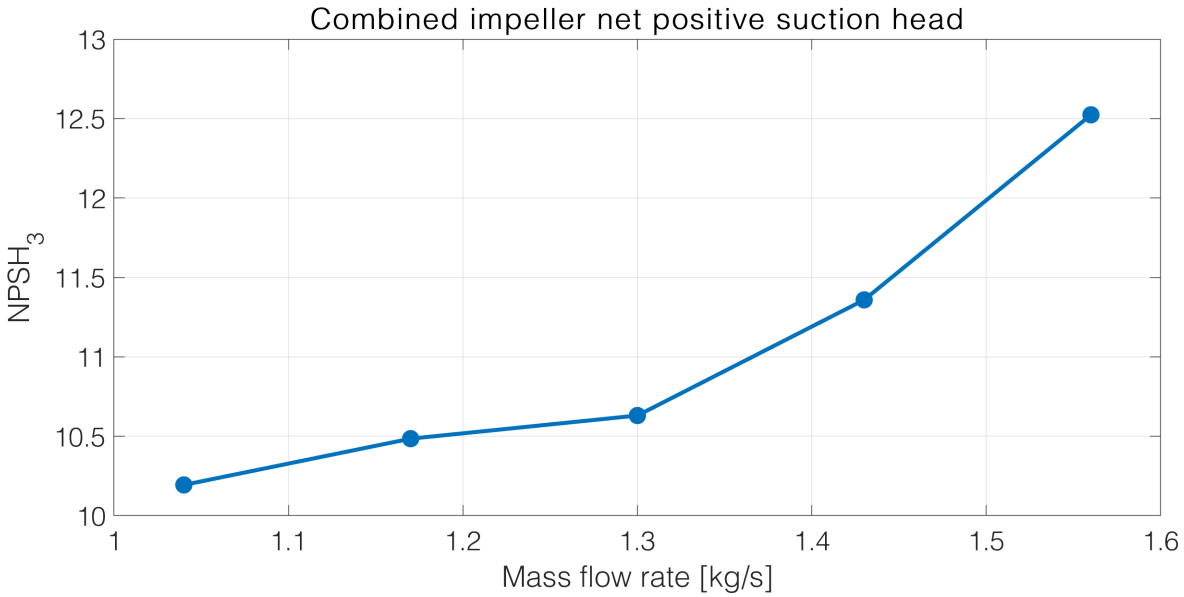

Figure 10.5: NPSH dependency on mass flow rate

Figure 10.6 shows the cavitation regions for the two-phase CFD simulation. The regions shown in green are more than 50 percent filled with the gaseous phase. It is interesting to note how large the cavitating region must be to significantly affect the delivery head of the pump. In general, the cavitation area is still located on the suction side of the leading edge of the blade. In particular, at the impeller inlet. However, a small cavitation region also exists on the leading edge of the splitter blades.

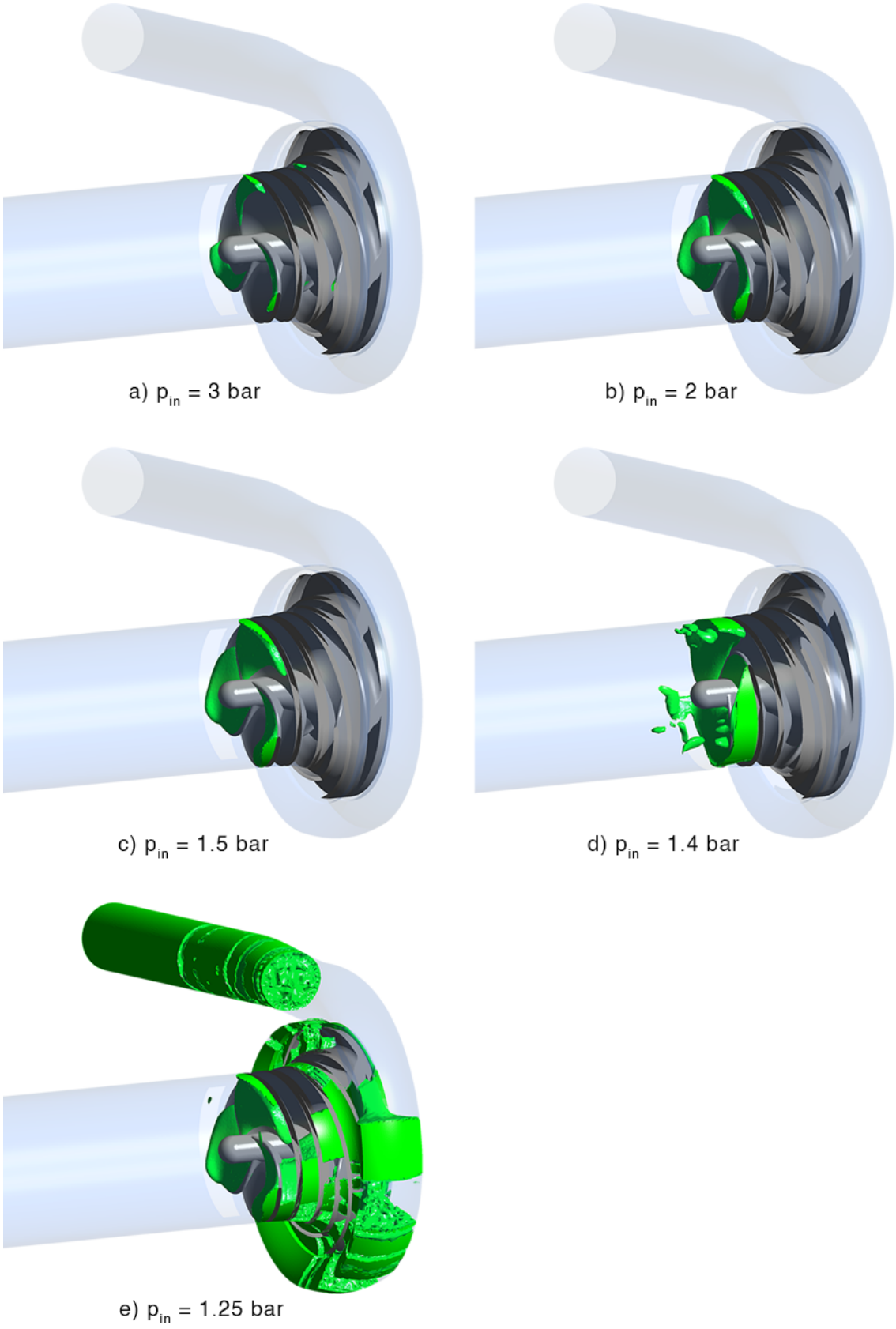

Figure 10.6: Cavitation presence at different suction static pressures

10.4 Open impeller effects

One of the goals of the thesis was to evaluate the construction of the impeller and the associated study of whether a cover disk is needed. From a hydraulic standpoint, a shrouded impeller is always more efficient than an open impeller. This is partly due to the absence of a rotating casing wall, which therefore cannot supply energy to the fluid in an open design, but mainly because the bypassing of the blades via the gap at the tip of the blades can be severe. This bypass results in a partial pressure equalization between the pressure and suction sides of the blade, which has an impact on the pump delivery head.

For this purpose, a series of simulations of impeller geometries with a modeled gap at the blade tip were performed. From the perspective of conventional impellers, the actual gap can be expected to have a thickness on the order of 0.2 millimetres. However, for a device of this small size, it is possible to reduce to this clearance as there is no large blade deformation or shaft deflection.

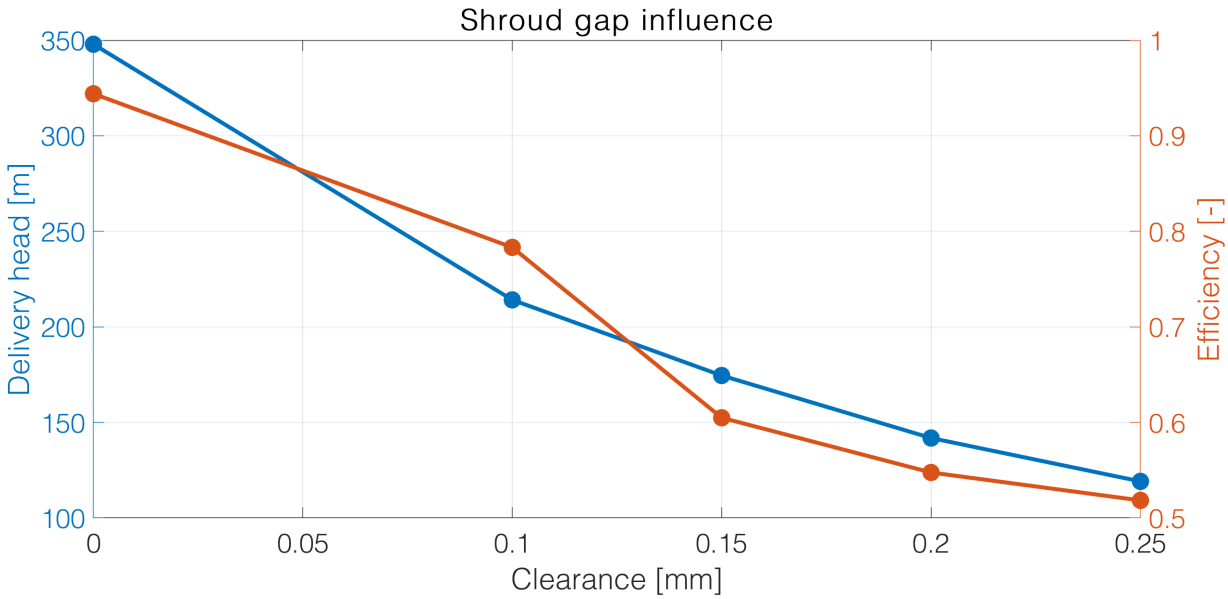

Figure 10.7: Blade tip gap influence on pump characteristics

Figure 10.7 shows the dependence of the delivery head on the blade tip gap size as well as its efficiency. It shows that a pump of this size is strongly susceptible to leakage around the blade edge. The discharge width of the impeller is about 1.5 millimeters, so a gap of 0.1 millimeter represents a significant portion of the flow channel. In addition, when the pump handles a large pressure rise over a small length, it implies a large pressure differential on the pressure and suction sides of the blade. This difference is compensated by leakage through the gap and the required delivery head cannot be achieved. Using a standard 0.2 millimeter gap size, the impeller delivery head drops by 61 percent compared to a closed design.

The blade tip gap seems to have a lower effect on impeller efficiency, as the required torque drops greatly with the drop in the delivery head. However, there is some drop in efficiency.

For a gap of 0.2 millimeters, the hydraulic efficiency drops by 39 percent. This drop is mainly due to the losses caused by the vortices at the blade tip.

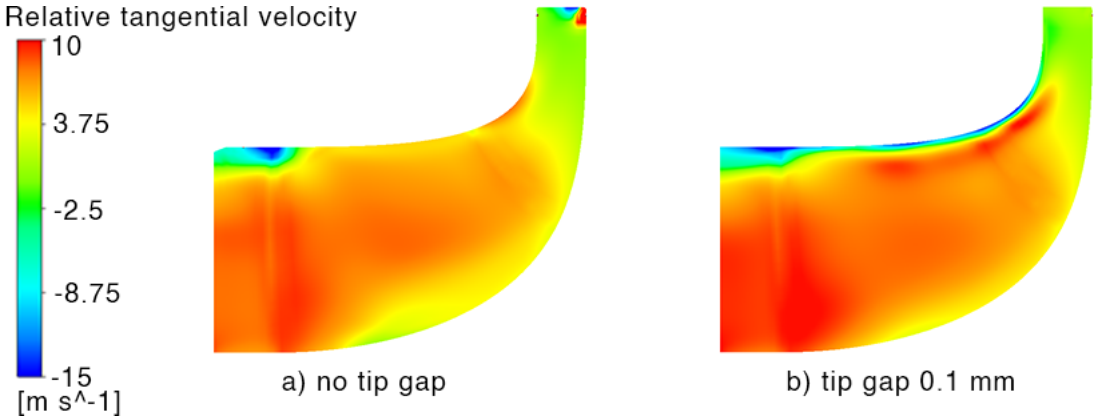

Figure 10.8: Relative tangential velocity distribution in closed and open impeller design

Figure 10.8 shows the difference between the flow inside an open and closed impeller design. The contour of mass-averaged tangential velocity value of the pump fluid is plotted onto the impeller meridian. There is a significant flow through the gap at the end of the blades, which compensates for the pressure difference on the pushing and suction sides of the blade. It is also possible to observe the formation of vortices at the end of the blades and their effect on the tangential velocity. There is a significant velocity difference, especially near the impeller housing, but the velocity is higher across the whole meridian. This is probably due to the vortices at the end of the blades reducing the active flow area and virtually decreasing the dimensions of the pump.

There was no simulation performed for this purpose, but it may be interesting to investigate the effect of the blade tip gap on the position of the optimum and the $Q - H$ characteristic. Given the velocity profile across the meridian, one would expect the optimum point of the pump to shift to lower flow rates as the gap size increases.

The open-wheel design is susceptible to the development of cavitation, as the vortices at the blade tips can create areas of low pressure, which can be hazardous in this application. Its blade recirculation, however, also lowers the pressure drop near the blade's leading edge, which can significantly lower the suction pressure required in some cases.

10.5 Structural analysis

A number of factors other than hydraulic properties determine whether the design of the impeller is feasible. In this thesis, the basic properties that could already make the current design unusable will be analyzed.

Using the finite element method, the mechanical stresses within the material and the risk of blade resonance occurrence will be analyzed.

10.5.1 Preprocess

The geometry is based on the same BladeGen model as the hydraulic analysis. However, for this model, the impeller hub and part of the electric motor shaft were also modeled in DesignModeller. To determine the stresses, it is important to note that the model contains rounded internal edges that match the actual part. Thus, a 0.2 millimeter fillet was modeled at the base of the blades.

The finite element method, like CFD, is based on the discretization of the geometry into many small elements, which is done by creating a computational mesh as shown in Figure 10.9. For the calculations, a model of the isotropic linear elastic material Inconel 718 is considered, whose properties are based on the Table 6.1.

The equations describing the stress distribution inside the material are analytically solvable and the quality of the mesh does not affect the stability of the solution, unlike CFD. However, the fineness of the mesh is important in terms of complex geometry representation and results interpolation. Therefore, a fine mesh was used in the critical locations. Because the transformation shapes are often complex, the interpolation is not always able to capture their shape sufficiently. As a result, the coarse mesh always exhibits higher stiffness, resulting in smaller deformations. It is commonly understood that for sufficiently realistic stiffness of thin-walled bodies, a minimum of three elements should be used across the wall thickness.

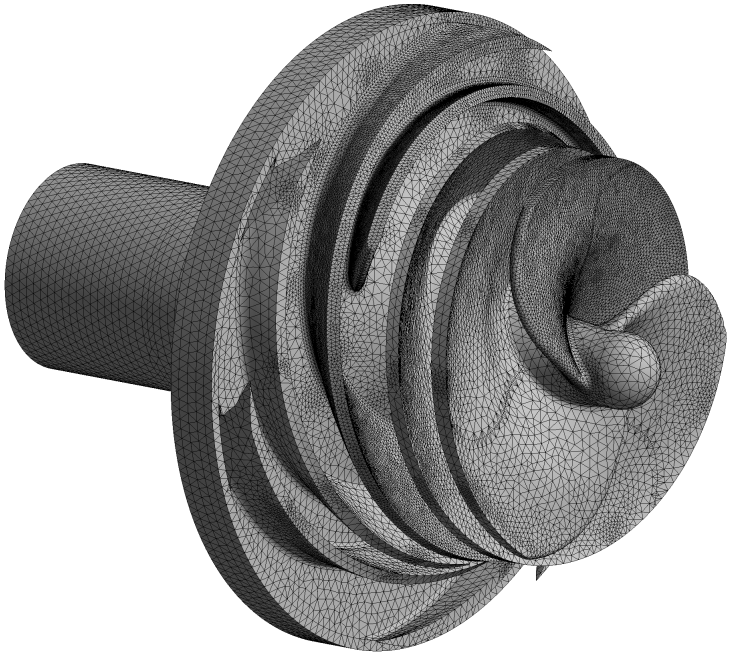

Figure 10.9: Impeller mesh for FEM analysis

For a sufficiently realistic stiffness of the component, an average cell size of 0.3 millimeters was chosen. The greatest load is expected to be on the blade passing around the tongue

of the spiral. This blade along with its fillet is therefore modeled using a finer mesh with a cell size of 0.15 millimeters.

The boundary condition geometrical definition can be seen in Figure 10.10. To calculate the stresses, the load from centrifugal acceleration due to the impeller rotation and the load from the pressure field of the fluid. The pressure distribution on the impeller surfaces was imported from the results of the previous CFD simulations. Component degrees of freedom were restricted using a fixed boundary condition on the shaft in the region underneath the bearing. This boundary condition prevents all displacements and rotations of individual elements.

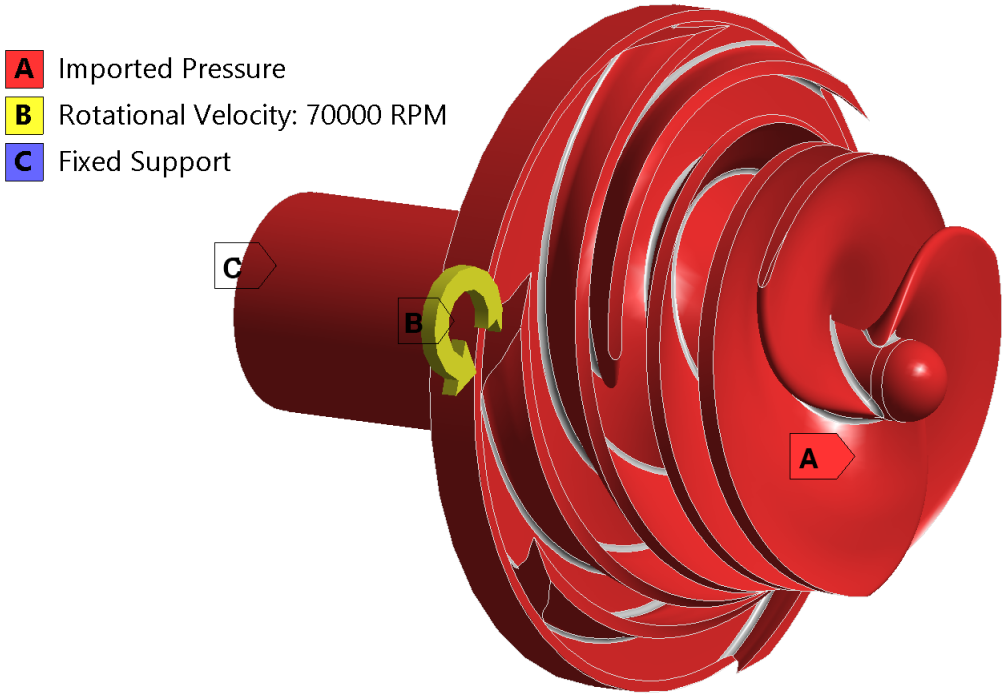

Figure 10.10: Impeller boundary conditions for FEM analysis

10.5.2 Structural stress

Most of the stress in the impeller is due to centrifugal acceleration at very high speeds and it was therefore necessary to determine whether the impeller could handle this speed. The stresses induced by the centrifugal forces are generally compensated by the back disc and its thickness needs to be designed accordingly. In this case, a thickness of 2 millimeters is sufficient as it does not induce stresses exceeding 30 megapascals (as is shown in Figure 10.11). This corresponds to the elasticity limit state safety factor of 34. Thus, there is a considerable room for geometry modification in this region to change the stiffness with respect to natural frequency manipulation.

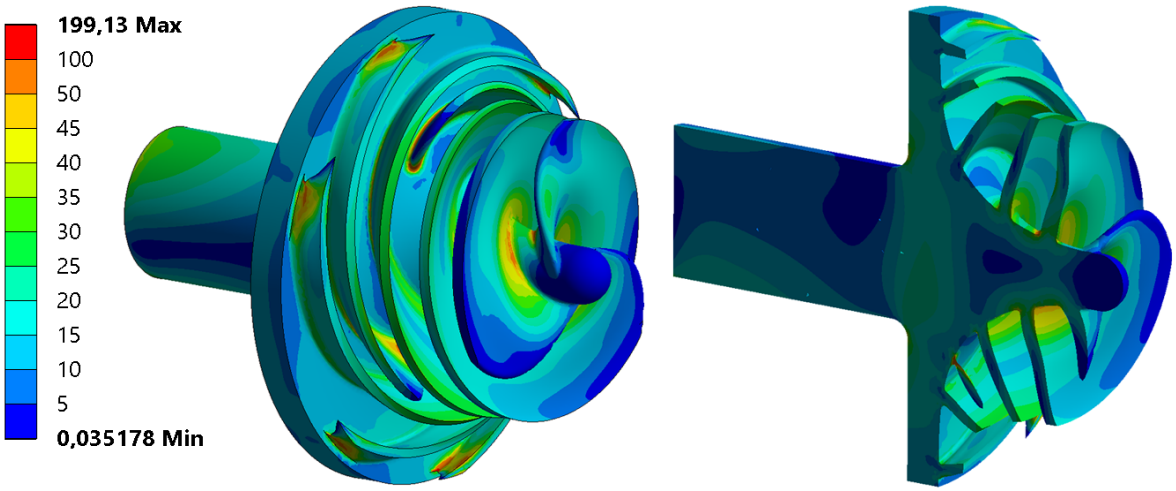

Figure 10.11: Equivalent (von-Mises) stress distribution in impeller

Centrifugal forces also act strongly on the blades, which are stressed by tension in the axial part of the impeller and by bending in the radial part. The greatest stresses on these blades are near their anchorage to the impeller hub. In addition, the blades are subjected to loads induced by the flowing fluid. Therefore, it is very important to have the fillet in the blade anchorage modeled correctly.

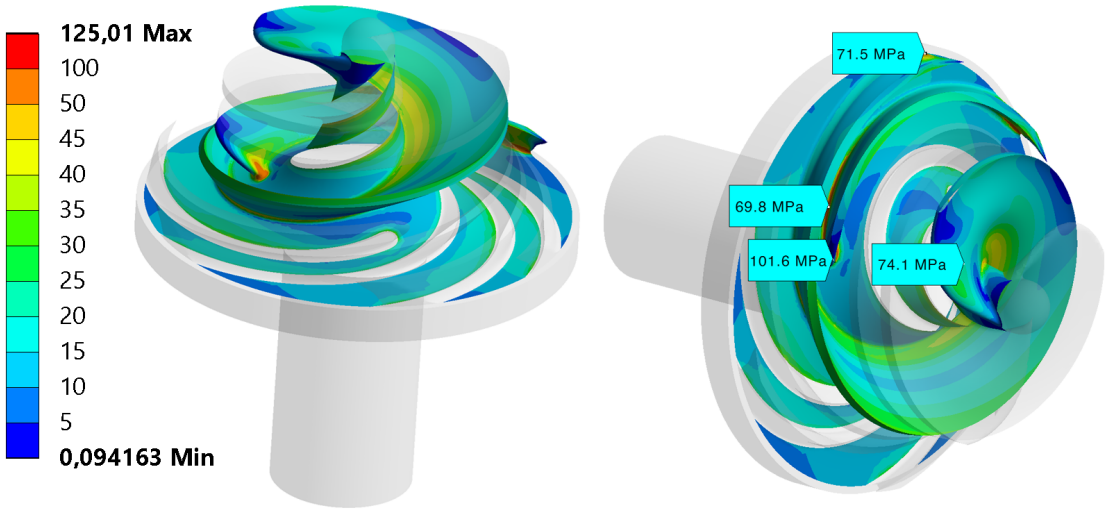

Figure 10.12: Equivalent (von-Mises) stress distribution on impeller blade

Figure 10.12 shows, that the highest impeller stress achieved is at the leading edge anchorage of the splitter blade, where it reaches a value of 101.6 megapascals. However, this stress is still relatively low and the elastic limit state safety factor is approximately 10 at this location.

Depending on the manufacturing technology, there is a possibility to reduce the blade thickness, which would potentially result in improved hydraulic properties.

10.5.3 Natural frequencies

As this design is a rotating machine operating at very high speeds, it is critical to ensure that such equipment does not operate near the resonance zone. Therefore, a modal simulation was performed to determine the impeller's natural frequencies.

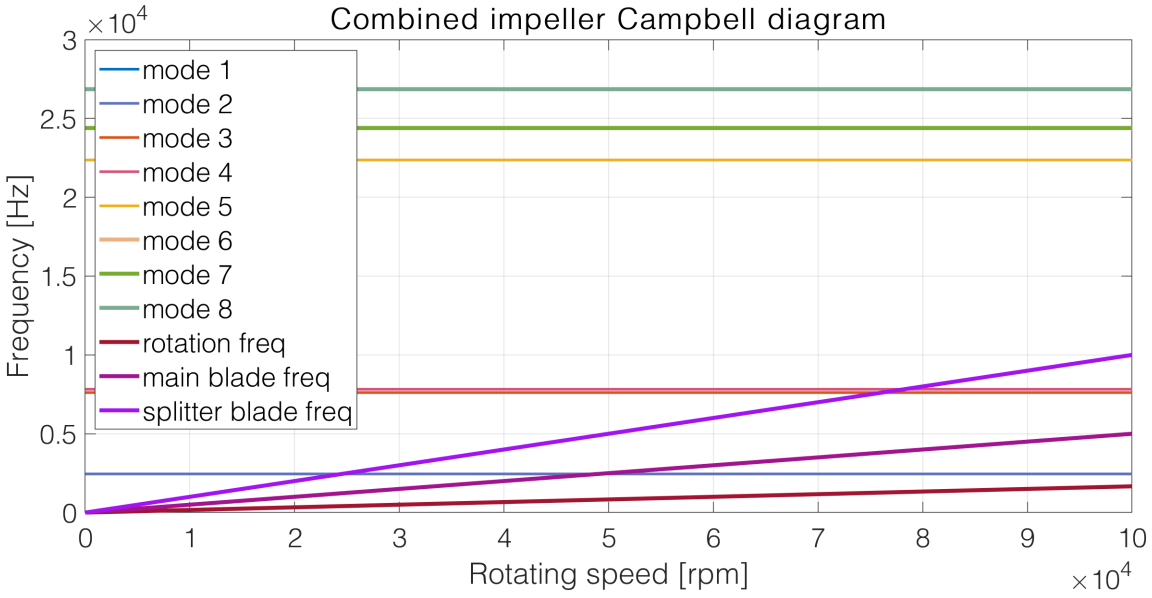

Figure 10.13: Impeller Campbell diagram

The simulation produced a series of natural mode shapes that the device is likely to exhibit, as well as the frequencies at which each shape will be amplified. Their overlaps with the excitation frequencies present in the impeller are plotted in Figure 10.13. The first 4 modes correspond to oscillations dependent on the impeller shaft mounting, the design of which was not the subject of this thesis and can therefore be expected to be avoided in future designs by changing the bearing locations or modifying the rigidity of the system. Modes six, seven, and eight are based on the oscillation of the individual blades and are therefore modes that are fixed by the impeller design. Fortunately, their frequencies are too high to be excited by rotor-stator blade interaction.

Chapter 11

Conclusion

The goal of this thesis was to develop a hydraulic design of an electric pump impeller for transporting an oxidizer to a rocket engine. The specific feature of this pump is that it must be able to operate at low inlet fluid pressure.

Weight is a very important parameter for rockets, as any added weight greatly increases work that must be exerted to transport the rocket to orbit. Weight can be reduced significantly in the area of the fuel and oxidizer tanks. Most oxidizer tanks are pressurized and need thicker walls to withstand this pressure as opposed to the pump proposed in this thesis, which is supposed to be able to operate at lower pressures so that the tanks can have thinner walls.

Therefore, a study of the currently used rocket engine concepts, their fuel, and the means by which it is being transported was carried out. The reasons that lead to the development of electrically powered fuel pumps were also presented. Finally, a concept design was presented, setting out the layout of the proposed pump into a functioning unit.

Since the main concern of the pump is to ensure cavitation-free operation, research was carried out to describe what cavitation is, why it occurs, and how it affects hydraulic machines. It is particularly important to mention where cavitation occurs so that it can be prevented. Relevant characteristics of centrifugal pumps working with cavitation present along with how they can be influenced during impeller design were presented.

In order for a potential impeller design to be actually usable, it has to be adapted to the capabilities of the manufacturing technology and the properties of the material used. Therefore, a study of the materials used for impeller production was carried out, from which Inconel 718 nickel superalloy was chosen to be used. This material is characterized by high corrosion resistance, erosion resistance, and high strength.

The radial stages of centrifugal pumps generally have the best efficiency. The first design of the pump impeller was, therefore, a radial stage that achieved the required parameters. The design is based on analytical and empirical relationships derived from methods and measurements applied in industry. This design also makes use of features that make it possible to increase its performance. In particular, the slanted trailing edge of the blades and the appropriate choice of the number of blades were meintioned.

Since a larger number of blades reduces the flow area, the meridional velocity increases, and the static pressure of the fluid decreases. The option to insert additional splitter blades

between the main blades in a region where the pressure is already sufficiently elevated to avoid the risk of cavitation was investigated. A variant with three blades and a variant with three additional splitter blades inserted between the main blades were then compared. It turns out that it makes sense to use more blades, as they ensure higher efficiency, given that there is less specific energy gain for each blade, which results in the blades not being that much overloaded. In addition, the impeller with more blades had a wider operating window depending on the different flow rates.

The problem with the radial impeller is the strong curvature of the fluid flow near the blade's leading edge. In this area, the fluid has low pressure and the curvature of the flow creates an area where the pressure drops even further, meaning that and strong cavitation can form in this area, which then disrupts the pump's operation.

This problem is typically solved by inserting the axial stage of the pump before the radial stage. The axial stage is less susceptible to the formation of a negative pressure region and will increase the pump pressure so that the radial stage can operate without difficulty. Again, several geometric features of axial pumps have been introduced to improve their efficiency and reduce the suction pressure required. These features were then used in the design. The inducer uses a slightly increasing hub diameter, which allows it to take advantage of the Coriolis acceleration of the fluid. The blades have a curved and slanted leading edge, which reduces the effect of the liquid boundary layer in the inlet manifold. In addition, the blade is shaped as an airfoil to allow more efficient fluid flow curving.

The geometries of the pump inlet and outlet were determined based on the separate design of the radial and axial impeller stages. The main goal of the thesis was to combine these two designs into a single unit and create an impeller that takes advantage of both designs. The design of the blades of this impeller was quite challenging, as both the axial and radial stages have rather complex blade geometries and considerable tuning of the pitch angle and wrap angle of the blades was required to ensure that they were properly mated. For each blade, these angles were defined in five layers.

The $Q-H$ characteristic was determined for the combined impeller, showing that the pump of the combined design achieves a higher maximum hydraulic efficiency, but has a significantly narrower operating window than the purely radial stage.

A two-phase simulation of the pump impeller was performed, which included the phase transformation of the fluid through cavitation. Using this calculation, the value of $NPSH_3$ was numerically determined as a function of the pump flow rate. The impeller was shown to be significantly less susceptible to cavitation than expected from the results of the single-phase calculation. The pump design is able to operate at an inlet pressure 27 percent lower than required.

Since the impeller has, due to the speed requirements, very small dimensions, its production is very limited. In particular, it would be problematic to maintain the required surface quality on the channel walls. Therefore, a feasibility study of an open impeller design was carried out for this design. A series of simulations were performed using geometries with different-sized gap sizes at the end of the blades. The results showed that the pump handles such a high-pressure rise over such a short distance that there is a very significant pressure difference on the pushing and suction sides of the vane. As the vane is only 1.56

millimeters high, a large amount of pumped fluid bypasses the blade from the pressure side to the suction side, causing the pump to lose a significant delivery head amount.

Finally, a structural stress analysis was performed to check the design against the elastic limit state and modal analysis to determine the design's susceptibility to resonant oscillation amplification. It showed that the impeller does not even approach the risk of plastic deformation and the blade's natural frequencies will not be excited during normal operation.

The resulting pump design is therefore applicable in the variant containing the cover disc. The $Q - H$ characteristic and the cavitation characteristic are known. The pump meets the required parameters and is also capable of operation in terms of stress and resonance. However, a problem arises with the open impeller variant, because in this case, the pump is not able to deliver the required delivery head if the gap at the end of the blades is greater than 0.1 millimeters. In this respect, the design requires further work, and the option of a cover disc being only used in the radial part of the impeller, with the axial part open, seems to be the most suitable option.

Bibliography

[1] Available at: www.pumpsandsystems.com/images/stories/Webinars/document1.pdf.

[2] *Cross-sectional-image-model*. Available at: inpraisesystems.cz/turbomachines-rotating-machinery/.

[3] *Struktura a Vlastnosti Materiálu*. Brno University of Technology, Faculty of Mechanical Engineering, Institute of Materials Science and Engineering. Available at: http://ime.fme.vutbr.cz/.

[4] *Useful information on pump corrosion and chemical compatibility*. Available at: https://www.michael-smith-engineers.co.uk/resources/useful-info/chemical-compatibility.

[5] *Handbook of astronautical engineering*. 1st ed.th ed. Koelle: Mc Graw Hill: 20150 55, 1961.

[6] *Inconel alloy 718*. 3200 Riverside Drive: Special Metals Corporation, 2007.

[7] *Handbook of Stainless Steel*. Riihitontuntie: Outokumpu Oyj, 2013. ISBN 978-0070491472.

[8] *A full range of impeller materials: Because wastewater doesn't come in standard*. 14125 South Bridge Circle: Xylem, Inc., 2015.

[9] *Launch Press Kit: Rocket 3.1*. 2020. Available at: https://astra.com/wp-content/uploads/2020/08/Rocket-3.1-Launch-Press-Kit.pdf.

[10] *Hydraulický návrh induceru palivového čerpadla pro raketový motor*. Brno, 2021. Masters thesis. Brno University of Technology, Faculty of Mechanical Engineering, Energy Institute. Available at: https://www.vutbr.cz/studenti/zav-prace/detail/129540.

[11] *Centrifugal Pump Impeller Material for Various Applications*. 2022. Available at: https://www.mecholic.com/2022/11/centrifugal-pump-impeller-material.html.

[12] Allison, C. B. *Hybrid and Decomposition Combustion of the Hydrazine Fuels: Contract NGR 39-009-077*. NASA Lewis Research Center, 1971.

[13] Babalola, P. O., Omada, J. E., Kilanko, O., Banjo, S. O. and Ozuor, O. Performance Evaluation of a Centrifugal Pump with different Impeller Materials. *Journal of Physics:: Conference Series*. IOP Publishing. 2019. DOI: 10.1088/1742-6596/1378/2/022091.

[14] Biheller, H. J. Radial Force on the Impeller of Centrifugal Pumps With Volute, Semivolute, and Fully Concentric Casings. *Journal of Engineering for Power*. july 1965, vol. 87, no. 3, p. 319–322. DOI: 10.1115/1.3678265. ISSN 0022-0825. Available at: https://doi.org/10.1115/1.3678265.

[15] Bláha, J. and Brada, K. *Příručka čerpací techniky*. Praha: ČVUT, 1997. ISBN 80-01-01626-9.

[16] Cherkassky, V. M. *Pumps, Fans, Compressors*. Moscow: Mir Publishers, 1984. ISBN 978-5030017488.

[17] David, T. *SpaceX's Mars rocket to be methane-fuelled*. 2012.

[18] Gegeoglu, K., Mehmet, K., Caglar, U. and Arif, K. Assessment of Using Electric Pumps on Hybrid Rockets. *Propulsion and Energy: Forum*. AIAA. 2019. DOI: 10.2514/6.2019-4124.
[19] Greatrix, D. R. *Powered Flight: The Engineering of Aerospace Propulsion*. Springer, 2014. ISBN 978-1-4471-2485-9.
[20] Gruntman, M. *Blazing the Trail: The early history of spacecraft and rocketry*. AIAA, 2004. ISBN 156347705X.
[21] Gülich, J. F. *Centrifugal Pumps*. Fourth editionth ed. Villeneuve, Switzerland: Springer Nature Switzerland, 2020. ISBN 978-3642128233.
[22] Hill, P. and Peterson, C. *Mechanics and Thermodynamics of Propulsion*. New York: Addison-Wesley, 1992. ISBN 0-201-14659-2.
[23] Hyun Duck, K., Sejin, K. and Chang Ho, C. Performance assessment of electrically driven pump-fed LOX/kerosene cycle rocket engine:: Comparison with gas generator cycle. *Aerospace Science and Technology*. Elsevier. 2018, no. 77. DOI: https://doi.org/10.1016/j.ast.2018.02.033.
[24] Jakobsen, J. K. and Keller, R. B. J. *Liquid rocket engine turbopump inducers:: Design criteria for liquid rocket engine turbopump inducers*. ID 19710025474.th ed. 1971.
[25] Kuentzmann, P. Introduction to Solid Rocket Propulsion. *NATO: Office National d'Etudes et de Recherches Aérospatiales*. 29, avenue de la Division Leclerc: [b.n.]. 2023, RTO-EN-023.
[26] Lubieniecki, M. J. *Rocket engine inducer design optimisation to improve its suction performance*. TU Delft, 2018. Masters thesis. Delft University of Technology.
[27] Makay, E. *Centrifugal Pump Hydraulic Instability: Research project 1266-18*. Pennsylvania 19067: Energy Research and Consultants Corporation, 1980.
[28] Moon, Y., Park, C., Jo, S. and Kwon, S. Design specifications of H2O2/kerosene bipropellant rocket system for space missions. *Aerospace Science and Technology*. Elsevier. 2014, Volume 33. DOI: https://doi.org/10.1016/j.ast.2014.01.006.
[29] Morrison, S. *The future of commercial space travel is almost here with the latest SpaceX launch: Elon Musk's private space company has now successfully launched two crewed flights into orbital space.* Available at: https://www.vox.com/recode/2020/5/26/21267533/elon-musk-spacex-demo-2-falcon-9-iss-manned-launch.
[30] Noskievič, J. *Kavitace v hydraulických strojích a zařízeních*. Vyd. 1th ed. Praha: SNTL - Nakladatelství technické literatury, 1990. ISBN 80-03-00206-0.
[31] Oliphant, K. LNG TRANSFER PUMPS:: IMPROVING OPERATION: HIGH SUCTION PERFORMANCE PUMP INDUCERS CAN ELIMINATE CAVITATION. *Turbomachinery International*. Available at: https://www.yumpu.com/en/document/read/33930045/pumps-lng-transfer-pumps-concepts-nrec.
[32] Oliphant, K. *Electric Pumps for Space Propulsion*. 2018. Available at: https://www.conceptsnrec.com/blog/electric-pumps-for-space-propulsion.
[33] Posch, G., Chladil, K. and Chladil, H. Material properties of CMT: metal additive manufactured duplex stainless steel blade-like geometries. *Weld World*. Springer. 2017. DOI: 10.1007/s40194-017-0474-5. ISSN 61:873–882.
[34] Rocket Lab USA, I. *Rocket engine thrust chamber, injector, and turbopump*.
[35] Sawka, W. N. and McPherson, M. Electrical Solid Propellants: A Safe, Micro to Macro Propulsion Technology. *Joint Propulison Conference*. AIAA. 2013. DOI: 10.2514/6.2013-4168.

[36] Sharon, J. *Characteristics of Centrifugal Pumps*. Rockwell Automation, 2012. Available at: https://www.pumpsandsystems.com/characteristics-centrifugal-pumps.
[37] Sloupenský, Z. *Návrh odstředivého čerpadla metodami diferenciální geometrie*. Brno, 2011. Dissertation. Vysoké učení technické v Brně, Fakulta strojního inţenýrství.
[38] Stejskal, J. *Analýza rychlostních a tlakových polí kapaliny, využitím křivočarých souřadnic*. Brno, 2017. Dissertation. Vysoké učení technické v Brně, Fakulta strojního inženýrství.
[39] Sutton, G. P. and Biblarz, O. *Rocket Propulsion Elements*. Ninth Editionth ed. New York: John Wiley & Sons, 2000. ISBN 0-471-32642-9.
[40] Sutton, G. P. *History of Liquid Propellant Rocket Engines*. AIAA, 2006. ISBN 978-1563476495.
[41] Teja, P. S., Sudhakar, B., Dhass, A. D., Krishna, R. and Sreenivasan, M. Numerical and experimental analysis of hydroxyl-terminated poly-butadiene solid rocket motor by using ANSYS. *Materials Today:: Proceedings*. Elsevier. 2020, Volume 33. DOI: https://doi.org/10.1016/j.matpr.2020.04.097.
[42] Versteeg, H. and Malalasekera, W. *An Introduction to Computational Fluid Dynamics: The Finite Volume Method*. Pearson Education Limited, 2007. ISBN 9780131274983.
[43] White, F. *Fluid Mechanics*. McGraw-Hill, 2003. McGraw-Hill series in mechanical engineering. ISBN 9780072831801.
[44] Wilfried Ley, W. H. *Handbook of Space Technology (Aerospace Series (PEP))*. 1st ed. 2009. ISBN 978-0470697399.
[45] Yang, L. Concept and Key Technology Analysis of Electric Pump-Fed Liquid Propellant Rocket Engine. *IOP Conference Series:: Earth and Environmental Science*. 2021. DOI: 10.1088/1755-1315/781/4/042016.